Performance Enhancement of a Thermoelectric Harvester with a PCM/Metal Foam Composite

Abstract

The present numerical investigation examines the performance improvement of thermoelectric generators (TEGs) by using phase change materials (PCM) and porous medium. Due to the high latent heat of PCMs, both sides of the TEG were filled with paraffin RT35 (on the cold-side) and paraffin RT69 (on the hot-side). The PCM in the cold-side of the TEG was used as a heat-sink whereas the PCM in hot-side of the TEG was used to reduce the output voltage fluctuations. Since the system was periodically subjected to heat flux from an external heat source, the paraffin in the hot-side of the TEG was also used to generate a continuous thermal heat when the heat source was cut-off. To increase the thermal conductivity of the phase change material, this investigation studied the effect of using the copper porous medium with different porosities (0.80, 0.90, and 0.95) and three different pores per inches (PPI) as 10, 20, and 40. The results show that the use of porous on the cold-side of the TEG produces more electrical energy and output voltage compared to (i) having porous medium on the hot-side and (ii) using PCM without porous medium on both sides of the thermoelectric generator. Furthermore, the results indicated that the TEG performance enhanced by increasing PPI and reducing porosity. As a result, by increasing the PPI from 10 to 40 (at 0.80 porosity) and by reducing porosity from 0.95 to 0.80 (at PPI 20), the electricity generated increases by 13.57 and 5.36%, respectively.

Keywords: Thermoelectric generator; Phase change material; Porous Medium; Numerical investigation; Heat-sink

1. Introduction

The 21st century commenced with concern about energy crisis. Increasing energy prices, declining fossil fuel resources, and escalating environmental concerns have quickly led to major policy changes in the energy sector. Fossil fuels have had an adverse impact on the environment. Greenhouse gas (GHG) emissions and the consequent global warming (GW) effect, melting ice glaciers, air pollution, and acid rain are just a number of threats that fossil fuels pose for the environment. There have been lots of efforts by scientists to reduce fossil fuel dependency. Thermoelectric generator (TEG) is the technology that can generate electricity directly from a heat source and it shows a great advantage compared to other existing technologies. Thermoelectric generators are widely used in many industries, i.e. medical applications [1], wireless sensors [2], electronic equipment [3], automotive engines [4], and space industries [5].

TEGs are highly applicable in industries due to numerous features such as direct power generation, high reliability, low maintenance requirements and they are environmentally friendly. Moreover, the heat sources are available naturally (solar or geothermal energy) or they can be achieved through industries heat waste (exhaust energy from vehicles) [6, 7]. However, in most of TEG's applications, the temperature boundary conditions are not stable. This is an important challenge to manage the efficiency and output power of the system which has a transient boundary.

Indeed, temperature fluctuations on both sides of the thermoelectric generator cause variations in power generation. Therefore, to design a thermoelectric generator, the system sustainability should be considered as well as increasing output power and efficiency.

In an experimental and modelling study, Guo et al. [8] proposed a new thermal management system which works based on thermal switches. The results obtained from this study shows that the proposed system is effective in reducing temperature fluctuations and increasing the output power of the system.

Mizuno et al. [9] used a thermal buffer system to reduce the temperature fluctuations of TEGs. These heat buffers are a combination of two alloys with high fusion enthalpy that is placed between the heat source and the thermoelectric generator. The results indicate the capability of the proposed system to control the stability of the generating power from TEGs.

Applying phase change materials (PCMs) is another method to control the oscillation of energy produced in thermoelectric generators. These materials can store large amounts of thermal energy in the form of latent heat within their melting and freezing points and they can be used as a viable option to mitigate the temperature variation. PCMs have unique properties such as high latent heat, thermal and chemical stability, lack of corrosion and high reliability. They are widely used in various industries such as energy storage [10, 11], air conditioning [12, 13], cooling system for electronic components [14, 15] and solar systems [16, 17]. Atouei et al. [18] carried out an experimental study on a two-stage thermoelectric generator in which, first, a thermoelectric generator was placed between the heat source and the heat sink filled by PCM and subsequently, in second stage, a heat sink with PCM was considered to be the heat source. The results of this study show that the power output of the double-stage system is 27% higher than the single-stage system. Also, by using PCM, the system can generate electricity when the heat source is cut off.

Another study has been conducted by Atouei et al. [19] is examining the effect of using PCM in controlling the hot and cold sides temperature of a thermoelectric generator. In this study, three different phase change materials with different properties (i.e. phase change temperature) were used in various configurations such as using (i) PCM on the hot-side, (ii) PCM on the cold-side and (iii) PCM on both sides. The results illustrate that by applying the phase change material in the hot-side of TEG, the fluctuation of output power reduces and the system can continue to generate voltage for some time after cutting off the heat source.

An experimental and modelling study by Tu et al. [20], presents a new PCM-based thermoelectric generator for space applications in which 5 to 10 wt% of expanded graphite was added to pure paraffin material to increase its thermal conductivity. The results of this investigation show that adding 5 wt% of expanded graphite has the significant effect on improving system performance. As a result, the output energy of the system increases by about 32% compared to that which was used pure paraffin as a phase change material.

Zhu et al. [21] also reported multi-parameter optimization based on using PCM in a thermoelectric generator system for space applications. They examined the effect of mass, phase change temperature and thermal conductivity of PCM as the main parameters in finding the optimal state. The outcome of the results shows that a phase change material with an appropriate phase change temperature produce a significant effect on the system power. The results also suggest that the maximum output power can be obtained when the phase change temperature is approximately equal to the average operating temperature of the system.

In an another study by Araiz et al. [22], the idea of using thermosyphon and phase change material as a transient heat exchanger in thermoelectric generators was examined. The results indicate that by using the proposed design on the cold-side of the thermoelectric, the power output of the system increases by 36% compared to using fin and forced heat convention.

Thermoelectric generators used in photovoltaic (PV) cells also have the issue of power fluctuations due to the variability of the intensity of the sun's radiation. In a numerical study, Cui et al. [23] examined the effect of using PCM on the hot side of the thermoelectric generators within the photovoltaic system and concluded that the use of phase change material is more efficient than single PV and PV-TEG.

Jaworski et al. [24] studied the effect of using phase change material as a heatsink on the cold-side of the thermoelectric generator for solar applications in which the results showed that the PCM has a high potential to improve thermoelectric generator performance.

Recently, Selvam et al. [25] conducted a numerical study to examine the thermal management of a thermoelectric generator using phase change materials. The results present the effect of PCM on different thermal fluids and suggested that using PCM on the cold-side of the thermoelectric controls its temperature and increases the thermal efficiency of the system within the range of 30 to 36.7%.

In the latest report by Liao et al. [26], a double PCM based thermoelectric harvesting was examined in which the system was placed in room temperature within the range of 0 to 40 °C for three days. The results show an increase in the average output power by 35.8% compared to a single PCM-based system.

Almost all previous studies unanimously reported that phase change materials can be used in thermoelectric generators in two different ways: (1) they can be used on the cold-side of the TEG as a passive system for temperature control, and (2) on the hot-side of TEG; since the boundary conditions are in transit condition, PCM can control the fluctuations of the generated voltage and, also, produce continuous voltage even when the heat source is cut off.

In this present numerical study, phase change material is being used simultaneously on both sides of the generator to achieve the above objectives. However, one of the major problems of using PCMs, is that they have a low heat transfer coefficient during the heat transfer. Therefore, a porous medium can be used to eliminate this problem [27]. Therefore, it can be argued that this paper, for the first time, is investigating the effect of the porous medium (with different porosity and PPI) on thermoelectric generator performance. The first part of this study examines three different scenarios to determine one which side of the TEG the porous medium with PCM should be used to have a more efficient thermoelectric generator. These scenarios were (i) no porous on both sides, (ii) porous in the hot-side of the TEG, and (iii) porous in the cold-side of the TEG. Subsequently, the second part explores and analyses the effect of porosity and PPI on system efficiency.

2. Geometry Model and Boundary Conditions

Fig. 1 shows the geometry model of this study which includes a thermoelectric generator, three copper plates, two PCM with different physical properties and a copper fin.

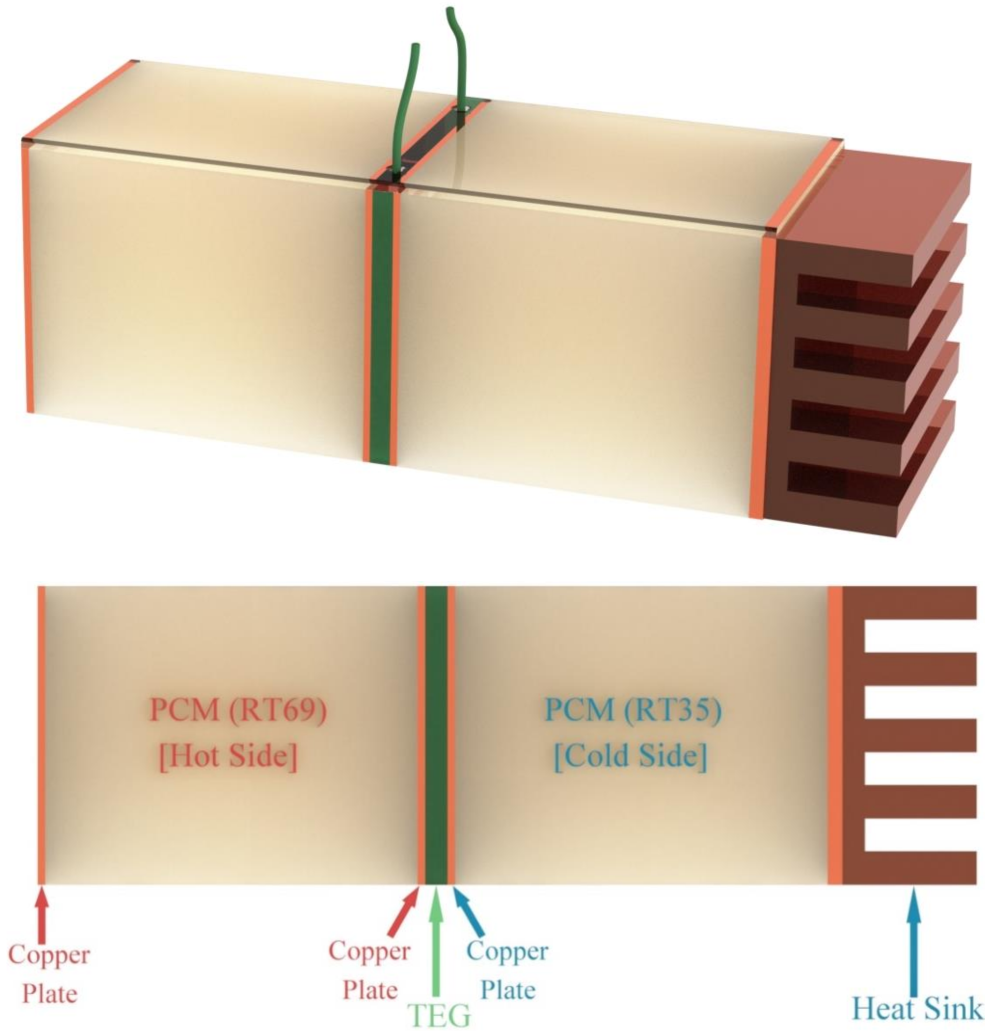

Fig. 1. schematic of the model

The dimensions of each part (thickness, width, and depth) are shown in Table 1:

Table 1
Dimensions of each part

	Number	Dimensions (mm^3)
Copper Plates	3	1*40*40
PCM Container	2	50*40*40
TEG	1	3*40*40
Air heat Sink	1	20*40*40
Number of fins	5	-
Fin thickness	-	4.5
Fin height	-	15

The physical properties of each material used in this investigation are also shown in Table 2:

Table 2
Materials properties used in the numerical calculation [21, 28]

		unit	PCM (RT69)	PCM (RT35)	Copper	TEG
Heat conductivity coefficient	k	W/m.K	0.2	0.2	400	2
Specific heat capacity	C_p	J/kg.K	2000	2000	385	154
Seebeck coefficient	α	V/K	-	-		0.035
Density	ρ	kg/m³	-	-	8920	7740
Solid density at 15°C	ρ	kg/m³	-	860	-	-
Solid density at 20°C	ρ	kg/m³	940	-	-	-
Liquid density at 45°C	ρ	kg/m³	-	770	-	-
Liquid density at 80°C	ρ	kg/m³	840	-	-	-
Melting range	T	K	341-343	302-309	-	-
Latent heat storage capacity	L	J/kg	230000	160000	-	-
Volumetric expansion coefficient	β	1/K	0.006	0.006	-	-
Prantl Number	Pr	-	38	38	-	-

As shown here, the heat conductivity coefficient (k) of both PCMs is extremely low. Therefore, to increase the system efficiency and utilising the maximum capacity of PCMs to store heat and energy, porous medium with different porosity and PPI were used. Table 3 shows different model configurations which were analysed in this study. These configurations consist of different arrangements as (i) PCMs on both side of the TEG without porous, (ii) there is a porous in the hot-side of TEG, and (iii) porous medium is located in the cold-side of TEG.

Table 3
Model configurations

	Name	Porosity (ε)	PPI
The PCM in two sides have not Porous	Case 1	-	-
The hot-side PCM has porous	Case 2	0.8	20
	Case 3	0.8	10
	Case 4	0.8	20
	Case 5	0.8	40
	Case 6	0.9	10
The cold-side PCM has porous	Case 7	0.9	20
	Case 8	0.9	40
	Case 9	0.95	10
	Case 10	0.95	20
	Case 11	0.95	40

As shown in Fig. 2, four sides of the system are insulated to avoid any heat transfer or heat loss.

$$\frac{\partial \mathrm{T}}{\partial \mathrm{y}} = 0 \tag{1}$$

The thermal energy with the rate of 50 watts enters from one side (hot) and exits from the opposite side (cold).

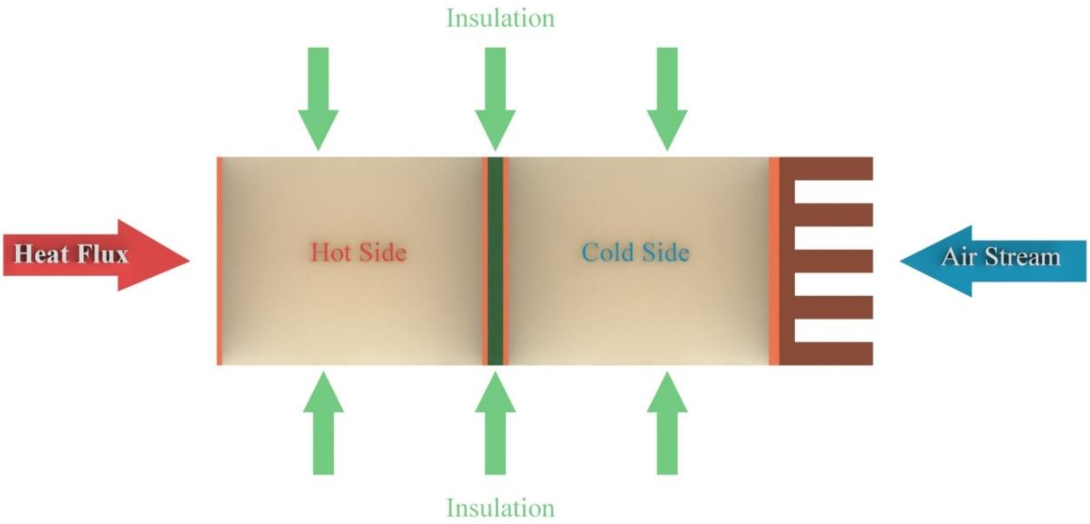

Fig. 2. Schematic of boundary conditions of the model

In order to meet the transient conditions, the system receives heat for 240 seconds in three different stages (see Fig. 3). The stopping time between each stage in which the thermal energy cuts off is about 180 seconds. The heat entering the system initially enters the first copper plate and it spreads rapidly, due to the high conductivity of the copper.

$$-k\frac{\partial T}{\partial n} = q'' \qquad (2)$$

Subsequently, it enters the hot-side of the system in which the PCM RT69 starts to melt. As shown in Fig. 1, there are three copper plates located within the system design. The first plate is placed at the entrance and the other two are positioned either side of the TEG. It should be noted that heatwave (generating from the melting processes) naturally tends to move upward within the PCM container. Therefore, copper plates with high conductivity are placed on both sides of TEG to conduct the homogeneous heat around the thermoelectric generator (heat in and heat out).

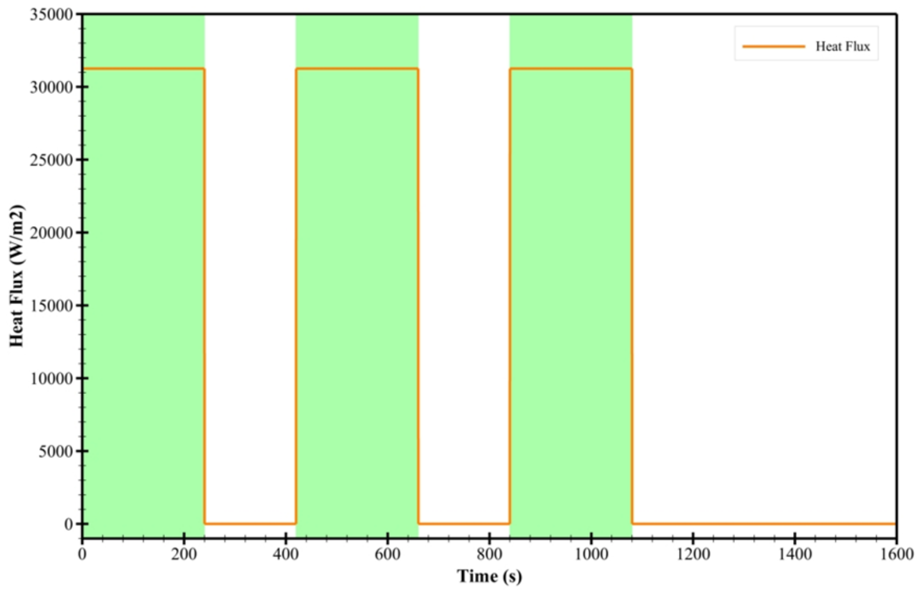

Fig. 3. The pattern of applying electrical power to the system

Finally, when the heat passes through the TEG and the third copper plate, it will enter the cold-side of the system and it starts to heat up and melt the PCM RT35 until it reaches to the copper fin or the heatsink. In this investigation and to reduce the temperature of the PCM used on the cold-side of the system, the heatsink is exposed to airflow rate at ambient temperature (298 K) and a heat transfer coefficient of 15 W/m^{2}K.

$$-k\frac{\partial T}{\partial n} = h(T - T_{amb}) \tag{3}$$

3. Assumption and Mathematical Model

3.1. Metal Foam / PCM Composite Formulation

The porous enthalpy method [29] for process simulation of phase change materials (PCMs) was used in this investigation. The following, therefore, were assumed for simulation:

- Flow in the melting section considered to be laminar, Newtonian and incompressible [30].
- A heatsink is the only way that system exposed to the environment and it has heat transfer with the ambient.
- The density change within the liquid phase that drives natural convection is only accounted for in the body force terms (Boussinesq approximation) in which variable density is defined as [31]:

$$\rho = \rho_0[\beta(T - T_0) + 1]^{-1} \tag{4}$$

Therefore, the density of the PCM in the other terms of the governing equations is assumed to be constant, which is the average of solid PCM density and liquid PCM density.

- Structure of the porous metal foam assumes as homogeneous, isentropic and open-celled [32].
- Conditions between PCM and porous medium considered to be as local thermal nonequilibrium.

Considering the above assumptions, the equations governing metal foam/PCM composite are as follows [33]:

Continuity:

$$\nabla.\vec{V} = 0 \tag{5}$$

Momentum in X-direction:

$$\bar{\rho}\left(\frac{\partial u}{\partial t} + V.\nabla u\right) = -\nabla P + \bar{\mu}\nabla^2 u + A_m u\frac{(1-\lambda)^2}{\lambda^3 + 0.001} - (\frac{\bar{\mu}}{K} - \frac{\bar{\rho}C_f|u|}{\sqrt{K}})u \tag{6}$$

Momentum in Y-direction:

$$\bar{\rho}\left(\frac{\partial v}{\partial t} + V.\nabla v\right) = -\nabla P + \bar{\mu}\nabla^2 v + \left(\overline{\rho\beta}\right)g(T - T_{ref}) + A_m v\frac{(1-\lambda)^2}{\lambda^3 + 0.001} - (\frac{\bar{\mu}}{K} - \frac{\bar{\rho}C_f|v|}{\sqrt{K}})v \tag{7}$$

Energy for PCM:

$$\overline{\varepsilon\rho C_P}\left(\frac{\partial T}{\partial t} + V.\nabla T\right) + \varepsilon\bar{\rho}L\frac{\partial \lambda}{\partial t} = k_{fe}\nabla^2 T + h_{sf}A_{sf}(T_f - T_s) \tag{8}$$

Energy for metal foam:

$$\varepsilon(\rho C_P)_S\left(\frac{\partial T_S}{\partial t}\right) = k_{se}\nabla^2 T_s + h_{sf}A_{sf}(T_s - T_f) \tag{9}$$

In all above equations subscript ‘f’ refers to fluid (PCM) and subscript ‘s’ refers to solid (metal foam). Velocities in x and y directions are shown with u and v, respectively. Moreover, T is temperature, μ is dynamic viscosity, P is pressure, C_P is specific heat, L is latent heat, ε is the porosity of the copper foam, K is permeability, C_f is the inertial coefficient, k_{fe} is the fluid effective thermal conductivity, k_{se} is the solid effective thermal conductivity, h_{sf} is inertial heat-transfer coefficient between liquid PCM and porous foam, and ρ is density.

In equations 8 and 9, A_{sf} is the specific coefficient surface area of metal foam which is calculated as the following [24]:

$$A_{sf} = \frac{3\pi\, d_l\left[1 - \exp\left(\frac{\varepsilon - 1}{0.04}\right)\right]}{(0.59\, d_P)^2} \tag{10}$$

A_m is also Mushy zone constant which is usually between 10^4 to 10^7 [34] and in this present study, it has been considered to be 10^6.

PCM liquid fraction (λ) is also described as:

$$\lambda = \begin{cases} 0 & T \leq T_s \\ \dfrac{T - T_{m,s}}{T_{m,l} - T_{m,s}} & T_s < T < T_l \\ 1 & T \geq T_l \end{cases} \tag{11}$$

Other parameters in Equations 5 to 11 are defined as follows: permeability (K), inertial coefficient (C_f), the fluid effective thermal conductivity (k_{fe}), the solid effective thermal conductivity (k_{se}). Furthermore, h_{sf} is the inertial heat-transfer coefficient between liquid PCM and porous foam.

3.2. Permeability and Inertial Coefficient

Characteristics of porous foam structure could be explained by variables such as porosity (ε), pore density (ω) and ligament diameter (d_l). These parameters [33] are:

$$\frac{d_l}{d_p} = 1.18\sqrt{\frac{1-\varepsilon}{3\pi}}\left[\frac{1}{1-\exp\left(\frac{\varepsilon-1}{0.04}\right)}\right] \tag{12}$$

Where,

$$d_p = \frac{0.0254}{\omega} \tag{13}$$

Other parameters of copper foam, i.e., permeability (K), inertial coefficient (C_f) are determined using formulations proposed by Calmidi and Mahajan [35]:

$$\frac{K}{{d_P}^2} = 0.00073(1-\varepsilon)^{-0.224}\left(\frac{d_l}{d_P}\right)^{-1.11} \tag{14}$$

$$C_f = 0.00212(1-\varepsilon)^{-0.132}\left(\frac{d_l}{d_P}\right)^{-1.63} \tag{15}$$

3.3. Effective Thermal Conductivity

Tian and Zhao [36] used following formulations for effective thermal conductivity of liquid PCM (k_{fe}) and effective thermal conductivity of porous medium (k_{se}):

$$\mathrm{k_{fe}} = \left.\frac{\sqrt{2}}{2(\mathrm{M_A} + \mathrm{M_B} + \mathrm{M_C} + \mathrm{M_D})}\right|_{\mathrm{K_{s=0}}} \tag{16}$$

$$\mathrm{k_{se}} = \left.\frac{\sqrt{2}}{2(\mathrm{M_A} + \mathrm{M_B} + \mathrm{M_C} + \mathrm{M_D})}\right|_{\mathrm{K_{f=0}}} \tag{17}$$

Where,

$$\mathrm{M_A} = \frac{4\sigma}{\left(2e^2 + \pi\sigma(1-e)\right)\mathrm{K_s} + \left(4 - 2e^2 - \pi\sigma(1-e)\right)\mathrm{K_f}} \tag{18}$$

$$\mathrm{M_B} = \frac{(e-2\sigma)^2}{(e-2\sigma)e^2\mathrm{K_s} + (2e - 4\sigma - (e-2\sigma)e^2)\mathrm{K_f}} \tag{19}$$

$$\mathrm{M_C} = \frac{\left(\sqrt{2} - 2e\right)^2}{2\pi\sigma^2\left(1 - 2e\sqrt{2}\right)\mathrm{K_s} + 2\left(\sqrt{2} - 2e - \pi\sigma^2\left(1 - 2e\sqrt{2}\right)\right)\mathrm{K_f}} \tag{20}$$

$$\mathrm{M_D} = \frac{2e}{e^2\mathrm{K_s} + (4 - e^2)\mathrm{K_f}} \tag{21}$$

$$\sigma = \sqrt{\frac{\sqrt{2}\left(2 - \frac{5}{8}e^3\sqrt{2} - 2\varepsilon\right)}{\pi\left(3 - 4e\sqrt{2} - e\right)}}, \text{and } e = 0.339 \tag{22}$$

3.4. Interfacial Heat Transfer Coefficient

One of the major problems in two-temperature models is a lack of interfacial heat-transfer coefficient between porous foam and PCM. In the current study, the interfacial heat-transfer coefficient between PCM and porous foam, h_{sf} is estimated using empirical equations provided by Zhukauskas [37]:

$$h_{sf} = \begin{cases} 0.76 Re_d^{0.4} pr^{0.37} \dfrac{k_f}{d_l} & 1 \le Re_d \le 40 \\ 0.52 Re_d^{0.5} pr^{0.37} \dfrac{k_f}{d_l} & 40 \le Re_d \le 10^3 \\ 0.26 Re_d^{0.6} pr^{0.37} \dfrac{k_f}{d_l} & 10^3 \le Re_d \le 2 \times 10^5 \end{cases} \tag{23}$$

$$Re_d = \rho \sqrt{u^2 + v^2} \frac{d_l}{\varepsilon \mu} \tag{24}$$

3.5. TEG Formulation

Based on the previous studies [20, 21, 38], the thermoelectric generation used in this study was assumed to be a uniform solid piece and the complexities of its internal geometry were not considered. Therefore, the figure of merits for TEG materials are identified as [21]:

$$ZT = \frac{\alpha^2 \sigma}{k_{TEG}} T \tag{25}$$

Where α, σ, k_{TEG} and T are the Seebeck coefficient, the electrical conductivity coefficient, the thermal conductivity coefficient, and the absolute TEG temperature. The maximum efficiency of TEG based on the terms Z and the temperature difference between the hot and cold sides of TEG ($\Delta T = T_h - T_c$) is identified as follows [21].

$$\eta_{TEG} = \frac{\Delta T}{T_h} \cdot \frac{\sqrt{1 + Z\overline{T}} - 1}{\sqrt{1 + Z\overline{T}} + \frac{T_c}{T_h}} \tag{26}$$

In the above relation, $\overline{T}$ is the average temperature of the hot and cold sides of the TEG. The maximum TEG output voltage and power can be obtained as [39]:

$$V = \alpha \Delta T = \alpha (T_h - T_c) \tag{27}$$

$$P_{max} = \frac{(\alpha \Delta T)^2}{4 R_{in}} \tag{28}$$

$$E = \int_0^t P \, dt \tag{29}$$

Where R_{in} is the internal electrical resistance of the thermoelectric generator. As mentioned before, in the present work, TEG is considered as a solid object. Therefore, the energy equation is the only governing equation.

$$\rho C_P \left(\frac{\partial T}{\partial t}\right) = k_{TEG} \nabla^2 T \quad (30)$$

4. Computational Details and Validation

ANSYS software was used in this study for the simulation analysis. The solver was set as pressure-based and transient for type and time, respectively. The SIMPLE method was, also, used to couple pressure-velocity governing differential equations [40]. The differencing scheme that was used to solve the momentum and energy equations was Second-Order Upwind whereas the PRESTO scheme was utilized for the pressure correction equation [41]. Residual convergence values were also set as continuity, 10^{-4}; momentum 10^{-5} and energy, 10^{-7}. The time step was, also, set as 0.04 second for all models.

The accuracy of the model in this study was examined with a comparison of the results with some similar experimental investigations. Since the present work includes simulation of the phase change materials (PCMs), thermoelectric generator (TEG) and porous medium, therefore two different studies were used to validate the simulation model developed in this investigation. An experimental work conducted by Tu et al. [20] was selected to simulate the thermoelectric generator and the phase change process. In this study, the hot-side of the thermoelectric is periodically exposed to a temperature of 100°C for 30 minutes and -50 °C for 3 minutes. The thermoelectric energy harvesting system used in this study is thermally insulated from the environment (Eq. 1).

Fig. 4 presents the comparison of temperature profile for the cold-side of TEG (T3) and the temperature of paraffin material (T5) at one point.

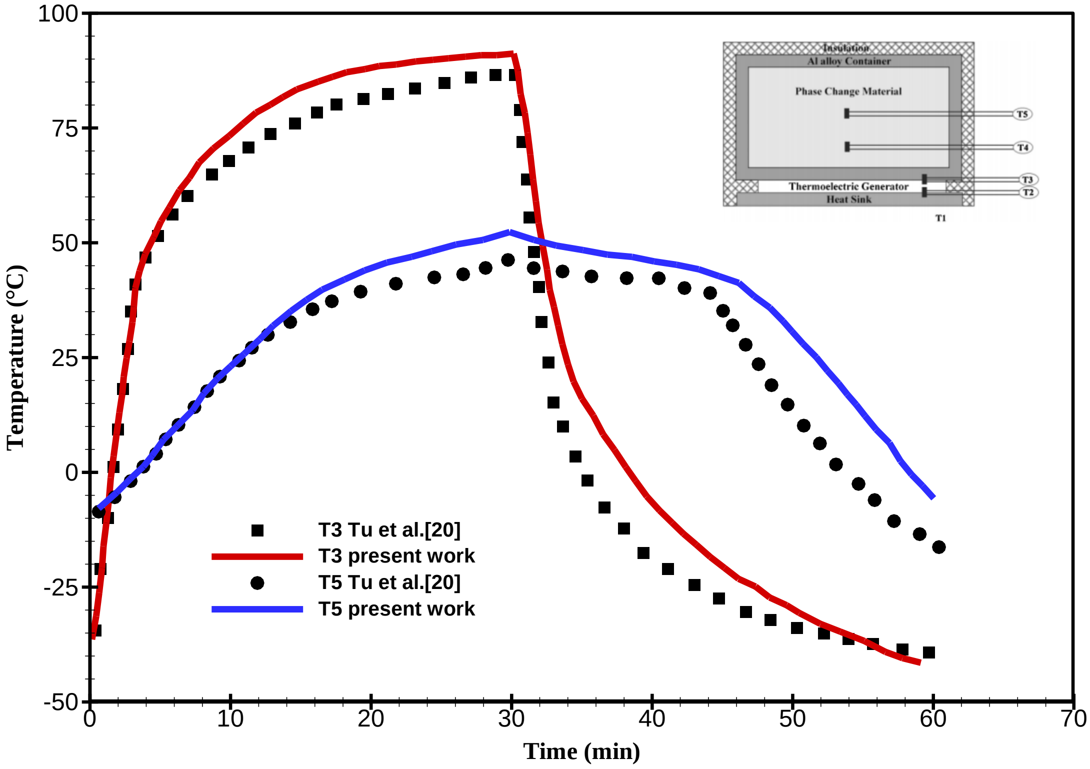

Fig. 4. Comparison of the temperature profile at different locations between present work and Tu et al. [20]

The validation of the simulation model with a porous medium was done by simulating the experimental study conducted by Zhang et al [42] in which they examined the melting process of paraffin composite and the metal foam in a cavity where there was a constant heat flux from one side of the system (Eq. 2). In this experimental study, the left wall is exposed to constant heat flux and other walls are exposed to natural convection (Eq. 3) and a copper foam with the porosity of 0.97 and PPI of 25 was used to act as a porous medium. Fig. 5 shows the result of the simulation model compared to the experimental data which presents an acceptable matching.

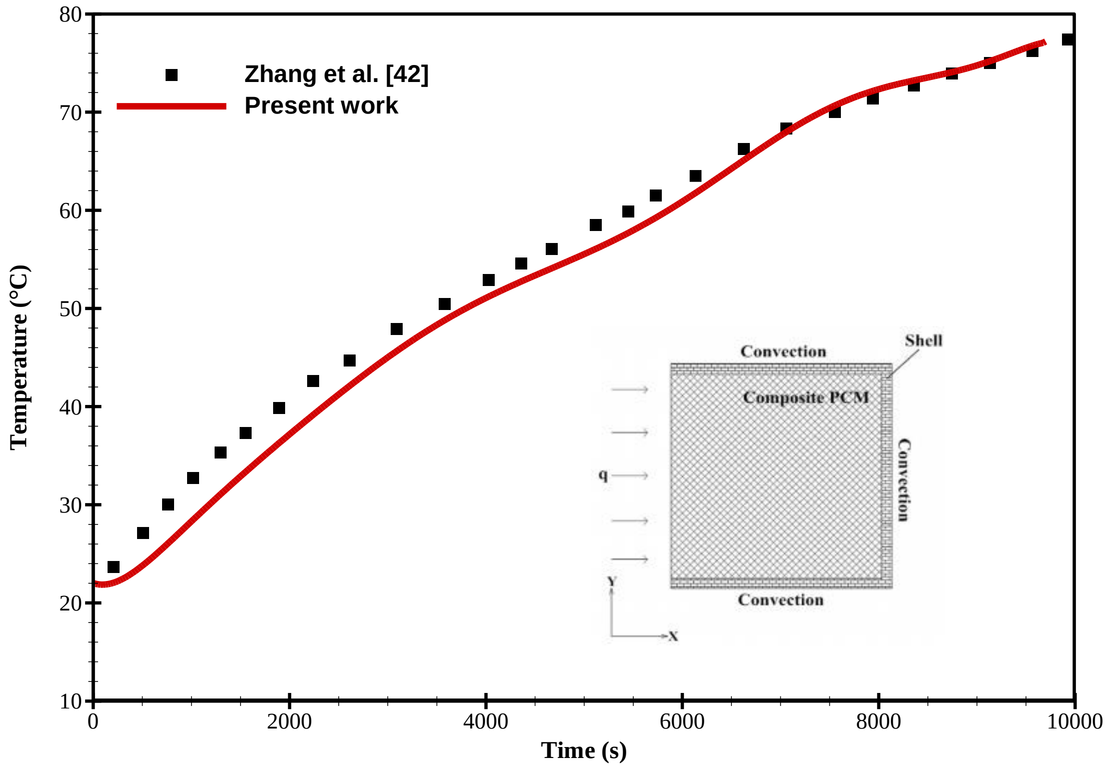

Fig. 5. Comparison of PCM temperature between the present work and Zhang et al. [42]

5. Results and Discussions

5.1. Identifying the Best Model Configuration

As mentioned previously, the first part of this study is to examine the effect of using a porous medium and its location on improving model performance. Therefore, cases 1, 2 and 4 are selected to be analysed first and their specifications are shown in Table 3. As it is shown, in Case 1, there is no porous medium in two sides of TEG while in other cases (2 and 4), the porous exists in different sides of the TEG.

Fig. 6 shows the graph of temperature difference on both sides of the TEG for the above cases.

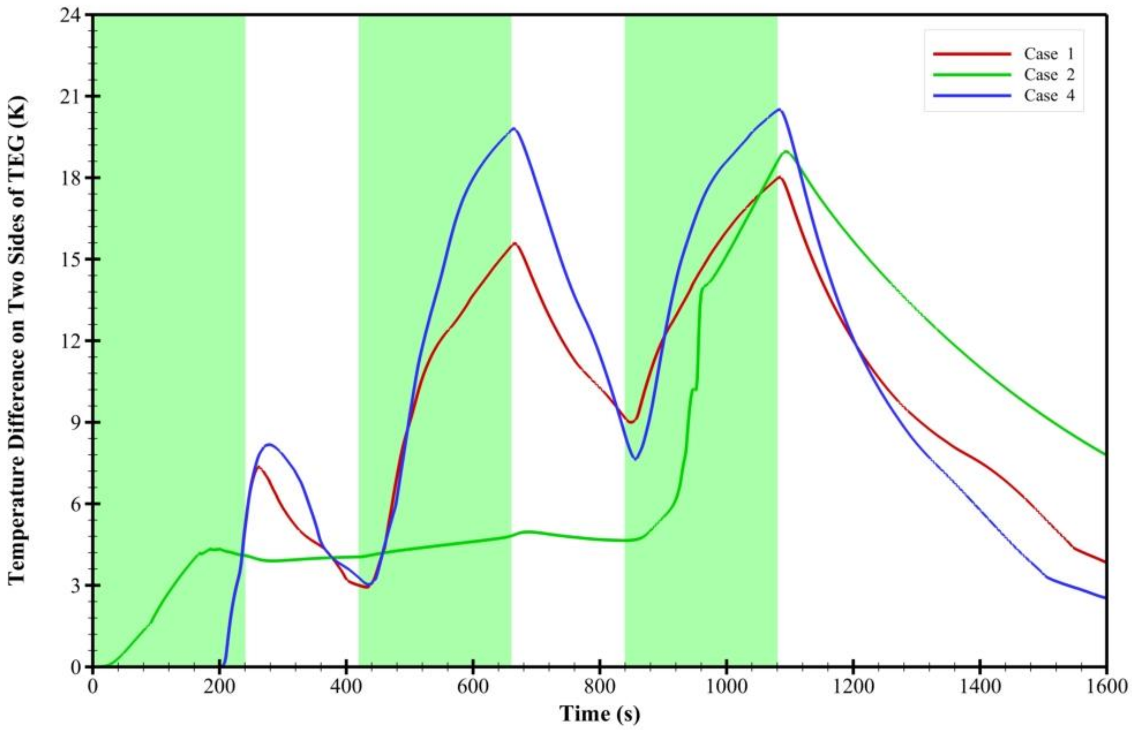

Fig. 6. Comparison of the temperature difference between two sides of TEG

As shown in this figure, two different behaviours can be claimed: (i) the starting point of the energy generation is different in these cases. In Case 2, the temperature difference started from the beginning of the process whereas in other cases, this begins almost at 200 seconds (slightly before the first heat cut-off), and (ii) the temperature difference profile in Case 2 is almost constant (about 5 K) within the first 880 seconds considering that the heat flux has been cut-off twice during this time. However, in the other two cases, the system had almost a proportional reaction with the heat supply.

In order to identify the suitable model for further investigations, the above claims have been analysed and the amount of energy produced by TEG has been calculated.

Claim-i can be referred to temperature contour profiles shown in Fig. 7 at 120 seconds. As shown, the temperature in Case 2 has increased across the hot-side of the TEG and it has reached to second copper plate located behind the TEG while in the other two cases, the temperature has increased, only, in some parts of the PCM. The reason for this behaviour is that, in Case 2, the PCM and copper porous are located on the hot side of the TEG and due to the high conductivity of the copper, the heat spreads quickly within its volume and reaches to the TEG. But in cases 1 and 4, the hot-side of the system contains PCM only and since the PCM conductivity is very low (see Table 2) therefore it takes longer for the heat to reach to the TEG.

Claim-ii can also be referred to as Fig. 7 and Fig. 8. As can be seen in these figures, due to the presence of porous in hot-side of the TEG in Case 2, the heat is homogeneously distributed throughout the PCM and it reaches to the second copper plate (before TEG) from the very beginning of the process. As shown in Fig. 8 at 240 seconds, the heat also penetrates through the PCM in cold-side of the model as well as melting some PCM. However, as shown in this figure, the melting heatwave in the other two cases is about to reach to the TEG at 240 seconds. Therefore, by analysing temperature and liquid fraction contours in Fig. 7 and Fig. 8, it can be concluded that the existence of porous in hot-side of Case 2, causes that more PCM in hot-side get involved during the heat transfer process and due to their physical properties (see Table 2) they can store more thermal energy in the form of latent heat. This functionality shows stability in the temperature difference on both sides of the TEG within the first 880 seconds of the process.

As it also is shown in Fig. 7, the maximum temperature in Case 2 is lower than the other two cases at different times. This is, again, due to the presence of the copper porous in hot-side of the TEG in which it can easily distribute the heat through the PCM and prevents heat to be trapped in the hot-side.

It is also clear that the porous in cold-side of the TEG in Case 4, has the same effects on the heat transfer of the model to the heat-sink and avoids the heat to stay longer in cold-side. As shown in Fig. 8 at 1000 seconds of this process, the heat spreads completely on the cold-side and it increased the PCM temperature which has melted the paraffin RT-35.

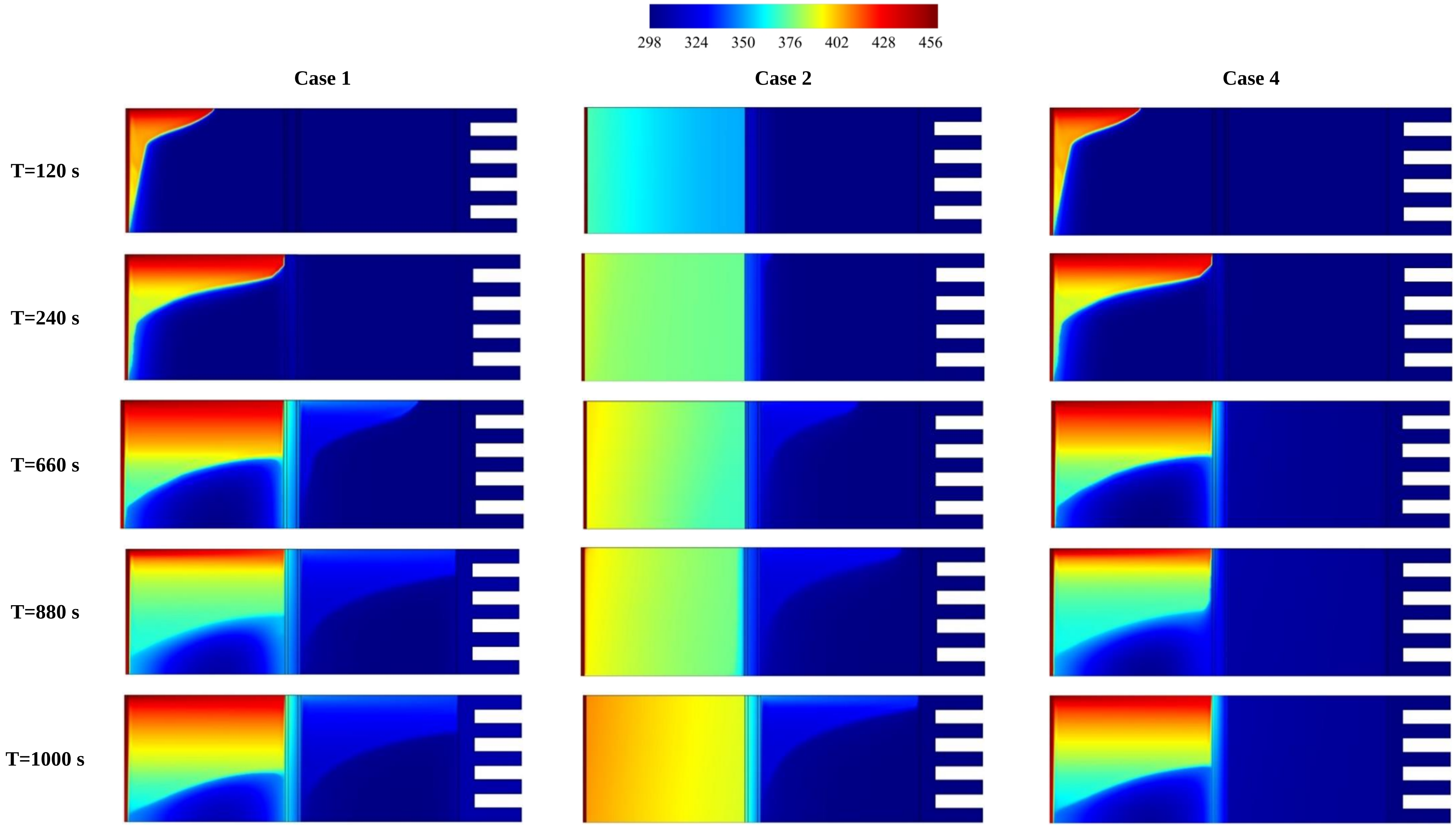

Fig. 7. Temperature distribution in three investigated cases

302

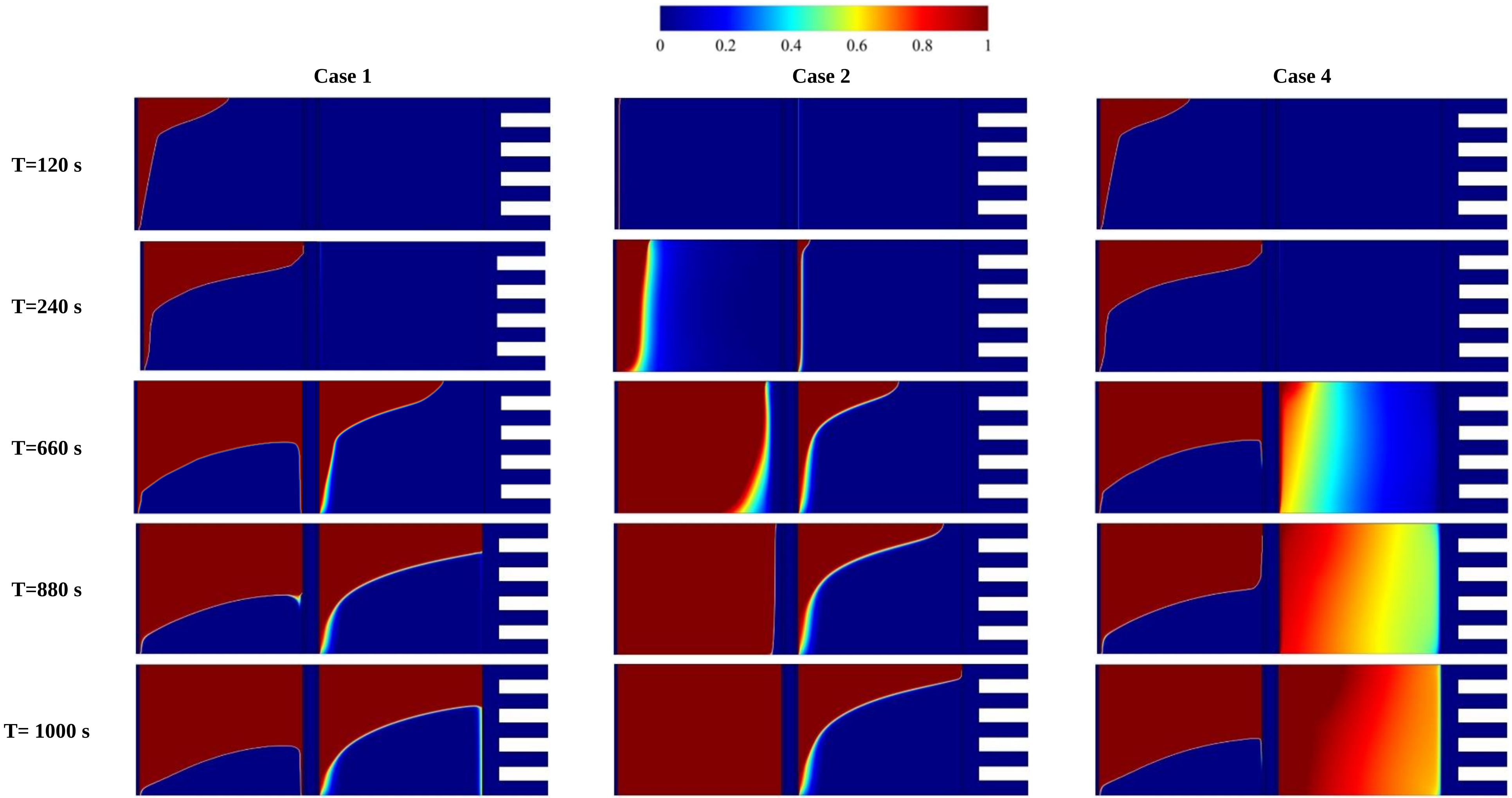

Fig. 8. Variation of Liquid fraction with time for five particular seconds

303

Fig. 9 shows the open-circuit voltage for the above cases (1, 2 and 4).

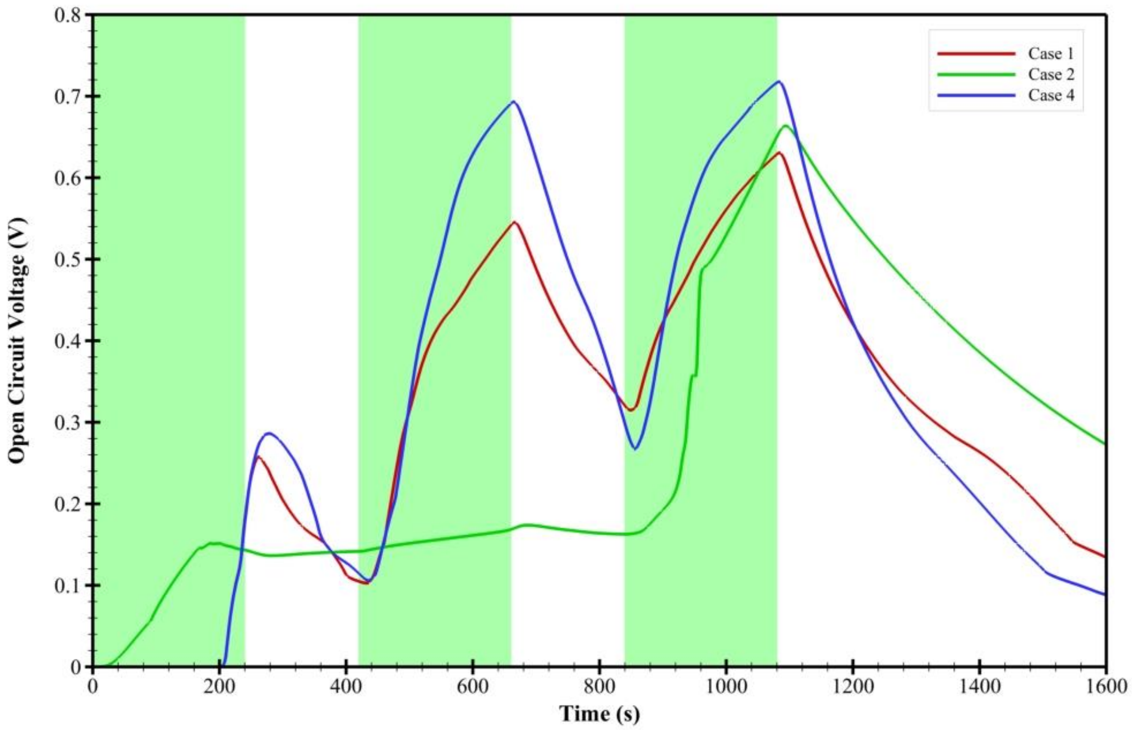

Fig. 9. Variation of electric voltage generation with time

Referring to Eq. (27), the output voltage is proportional to the temperature difference between both sides of the TEG. As shown in this figure, the output voltage, at each stage, increases by using the porous in cold-side of the TEG, whereas the existence of the porous in hot-side of the TEG (Case 2) it reduces the voltage. It is also observed that over time, by turning on and off of the heat source, the voltage in all cases increases.

Fig. 10 shows changes in electrical power generated by TEG for the three cases studied in the first part of this investigation.

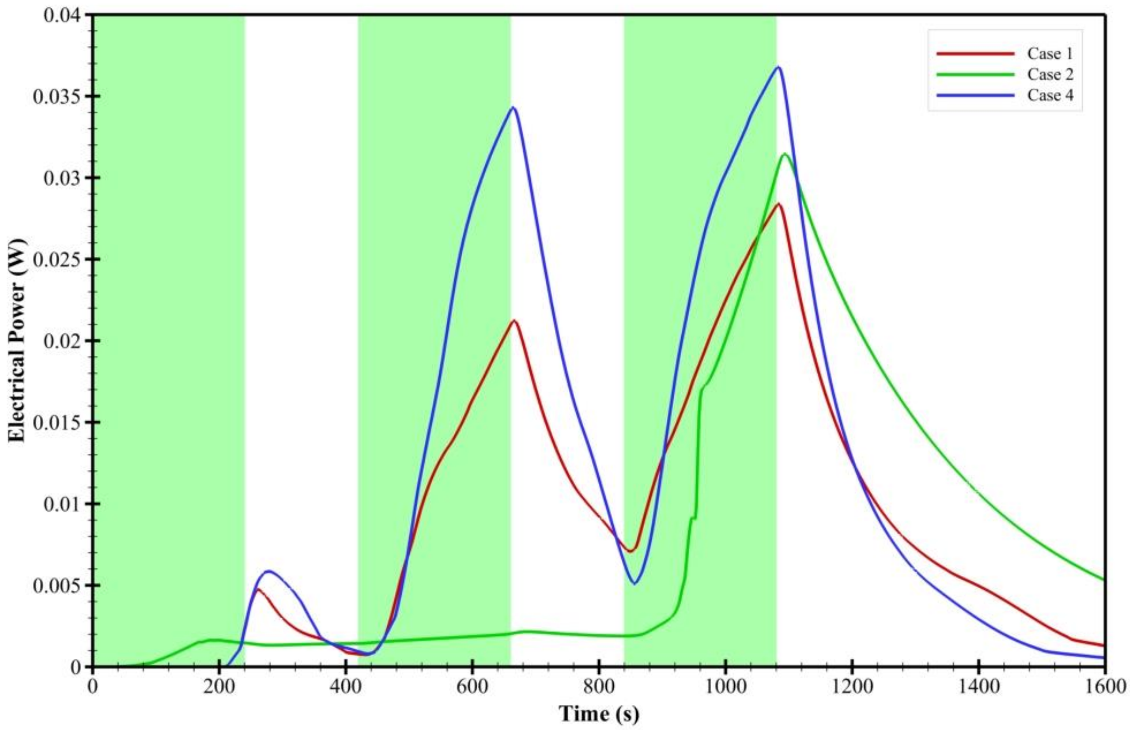

Fig. 10. Variation of thermoelectric maximum electrical power with time

As can be seen in this figure, over time, by turning on the heat source and transferring the heat through the system, the electrical power generated in Case 4 significantly increases compared to the other two cases. This is due to the effect of PCM (paraffin RT69) in the hot-side and its capability of storing heat and using porous in the cold-side of the TEG and its high heat transfer coefficient to the heat-sink and cooling the PCM (paraffin RT35). These cause that in Case 4 the temperature difference between both sides of the TEG becomes greater compared to the other two cases and as a result, generates more electrical power.

Further analysis in comparing the trend of electrical energy produced by the TEG shows in Fig. 11.

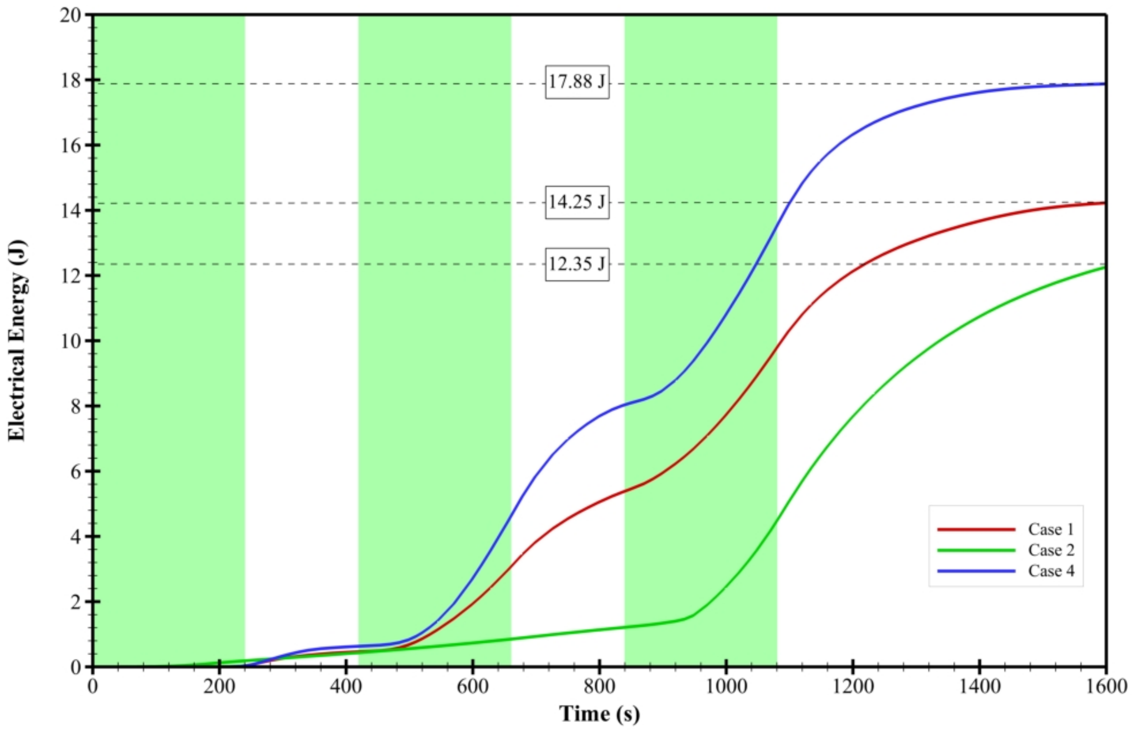

Fig. 11. Variation of thermoelectric electrical energy generation with time

As can be seen in this figure, it can be concluded that all the above arguments in comparison of these cases are accurate and Case 4 (with porous in cold-side of the TEG) is a better model compared to cases 1 and 2. If the electrical energy produced by each case can be stored in a rechargeable battery, as shown in Fig. 11, Case 4 can store 25.5% more than Case 1 and 44.8% more compared to Case 2. Therefore, in an emergency, any device (i.e. a sensor) connected to this battery has a longer time to utilise the stored electrical energy.

Therefore, according to all these analyses, it can be determined that the model used in Case 4, because of the capability of hot-side PCM in storing heat and positive effect of porous in transferring heat from cold-side PCM to heatsink and as result more temperature difference in two sides of its TEG and producing more electrical energy, is better and more efficient than the other two cases and utilised as the base model for other studies. Therefore, the following sections will discuss cases which are using porous (with different porosities and PPIs) in cold-side of the TEG.

5.2. Effect of Changes in Porosity and PPI

This Section shows the analysis of the other cases (3 to 11) which have the same model geometry as Case 4. These analyses include the effect of changes in porosity (0.80, 0.90, and 0.95) and PPI (10, 20, and 40) in porous which is located in the cold-side of the TEG.

5.2.1. TEG Performance with Changing of PPI at Constant Porosity

Fig. 12 shows the variation of the average temperature of PCM and the amount of paraffin melted on both sides of the TEG for the porosity of 0.80 and different PPIs (cases 3, 4, and 5).

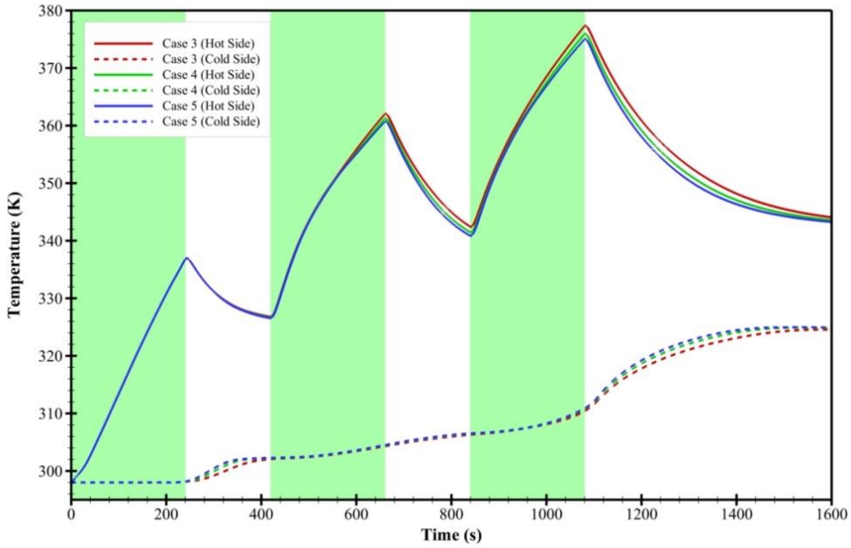

(a)

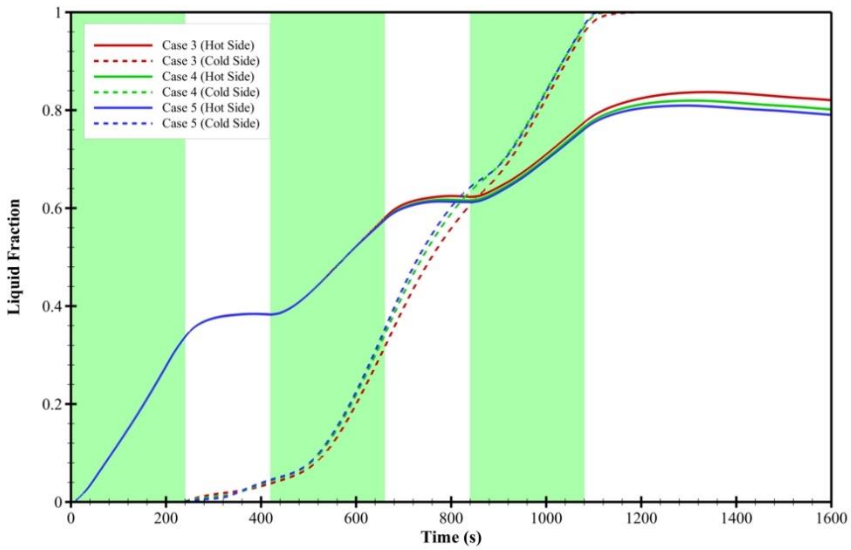

(b)

Fig. 12. (a) Variation of the average temperature of PCM with time (b) Variation of the liquid fraction of PCM with time

As shown in Fig. 12(a), by increasing the PPI the average PCM temperature decreases in hot-side of the TEG but it raises within the cold-side of the TEG. Fig. 12(b) also shows the variation of the liquid fraction of PCM over time. As it shows, the liquid fraction in cold-side of the models is increasing constantly. However, in hot-side of the TEG, the liquid fraction had a fluctuated trend over time. This is because that when the heat source is inactivated, the hot-side PCM acts as a heat source and uses the stored heat energy to continue generating electricity, thus the melting process stops.

Fig. 13 also demonstrates the variation of heat flux from the cold-side PCM to the heatsink.

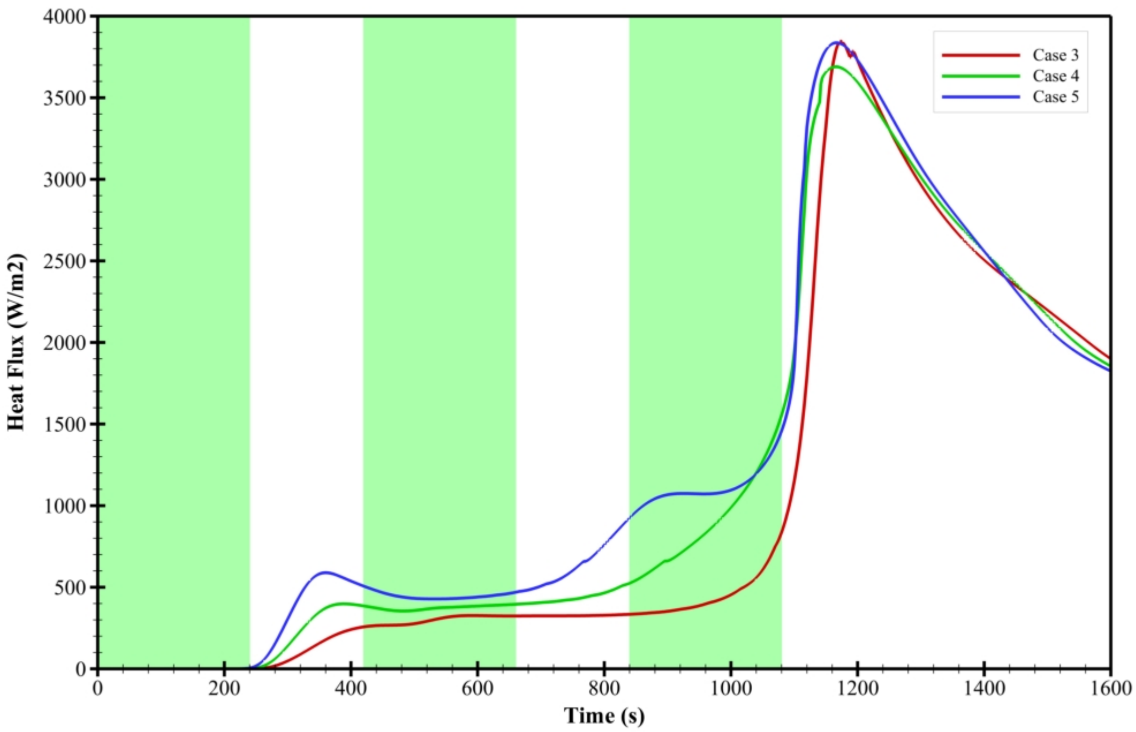

Fig. 13. Variation of heat flux from cold-side PCM to heat-sink with time

As shown in this figure, by increasing the PPI in the porous medium, the amount of heat flux increases from the cold-side PCM to the heatsink. This is because that by increasing the PPI, actually the common surface between porous medium and PCM is increased and as result, the rate of heat transfer from PCM to porous medium and then, to the heat-sink will be increased.

This heat flux behaviour is also similar for the cases with 0.90 porosity (cases 6, 7, and 8) and 0.95 porosity (cases 9, 10, and 11).

The temperature profile and the temperature difference between both sides of TEG in cases 3, 4 and 5 with a porosity of 0.80 are shown in Fig. 14.

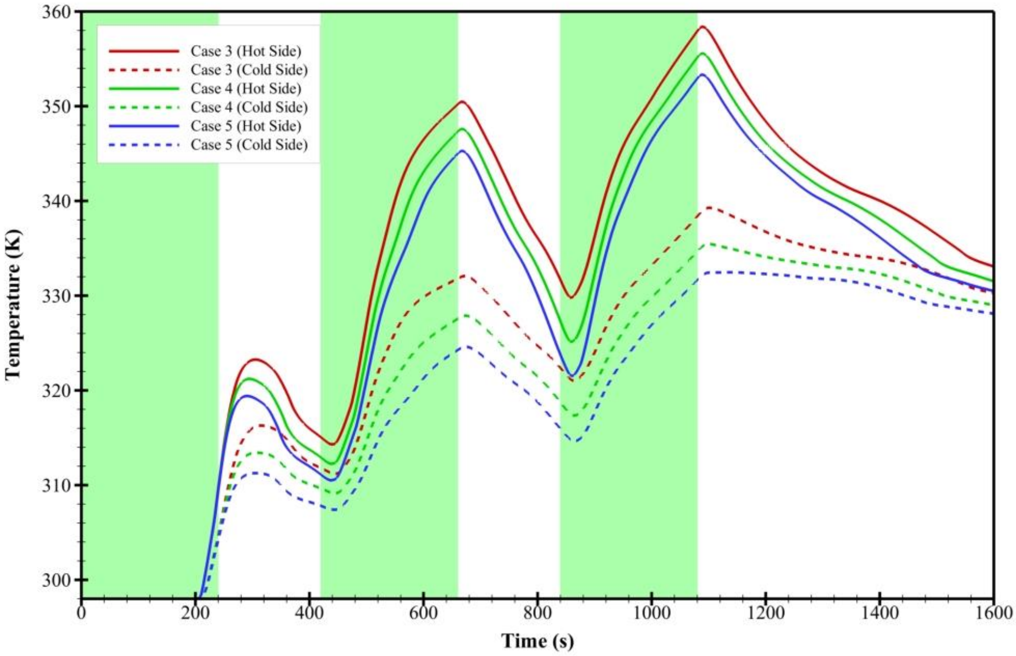

(a)

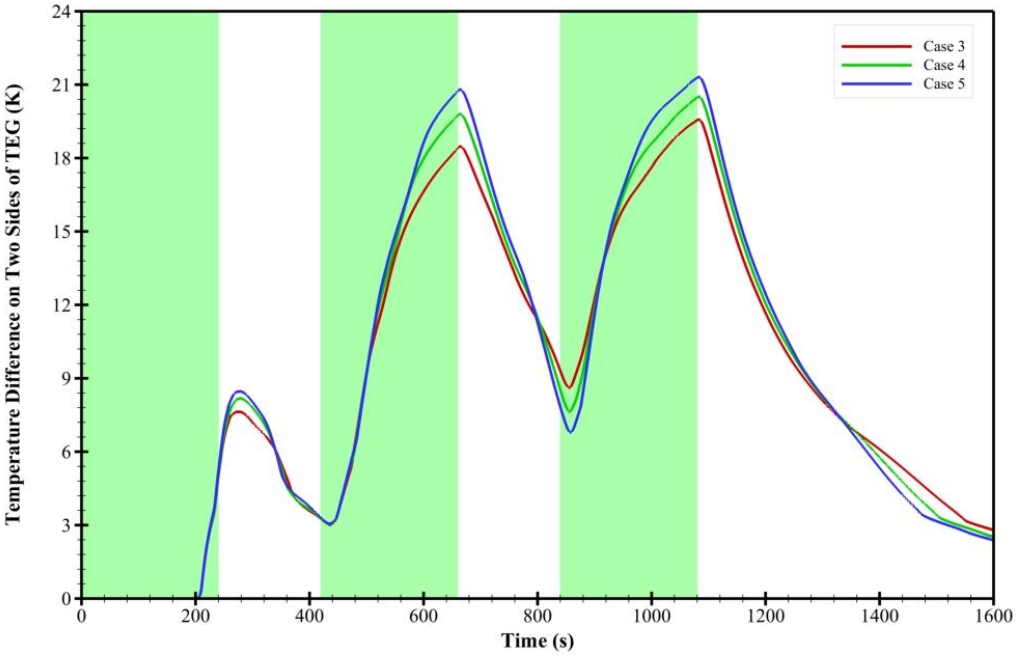

(b)

Fig. 14. Comparison of temperature and its differences between two sides of TEG

As a result, when PPI increases, the temperature of the hot-side and the cold-side surfaces of the TEG decreases, but the temperature difference between them increases. This is because, when PPI increases, in fact, the contact surface area between the copper porous and paraffin material increases, thus more amount of thermal energy stored in cold-side PCM will be transferred to copper porous and subsequently discharged to the heat-sink.

Fig. 15 shows the open-circuit voltage in TEG and as can be seen, the trend of its changes is similar to the graph of temperature difference in Fig. 14(b). It is also observed that as the input thermal heat to the system increases, the voltage output increases with increasing PPI.

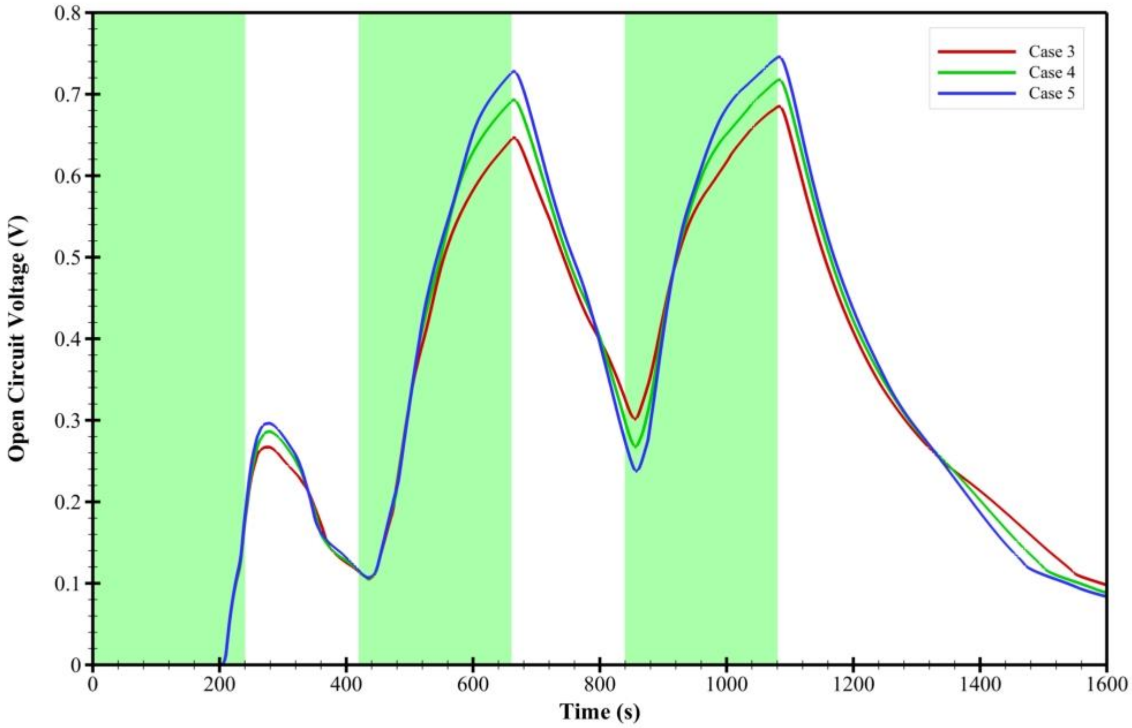

Fig. 15. Variation of electric voltage generation with time

Moreover, Fig.16 presents the variation of electrical power and electrical energy produced by TEG in cases 3, 4 and 5 with a porosity of 0.80. It is quite evident that by increasing PPI, the amount of electrical power and energy increases. As shown in Fig. 16(b), by increasing PPI from 10 (Case 3) to 20 (Case 4) the amount of energy produced by TEG raises by 7.88% and with the further increase of PPI to 40 (Case 5), the energy production will be increased by 13.57%, respectively.

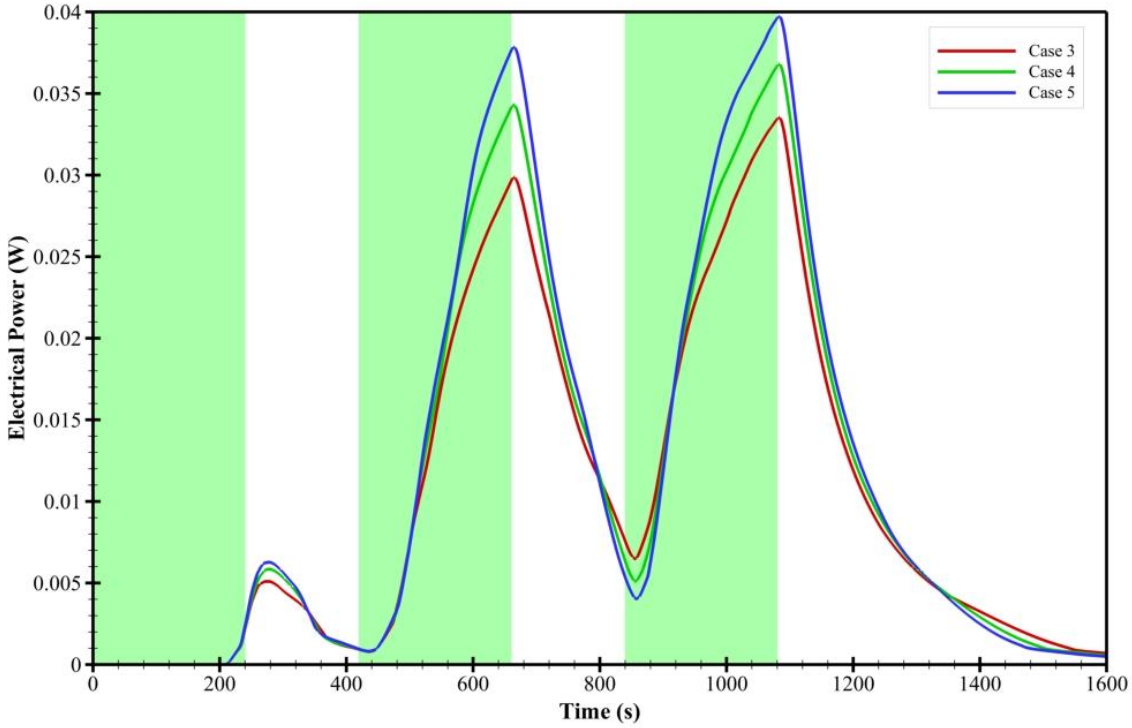

(a)

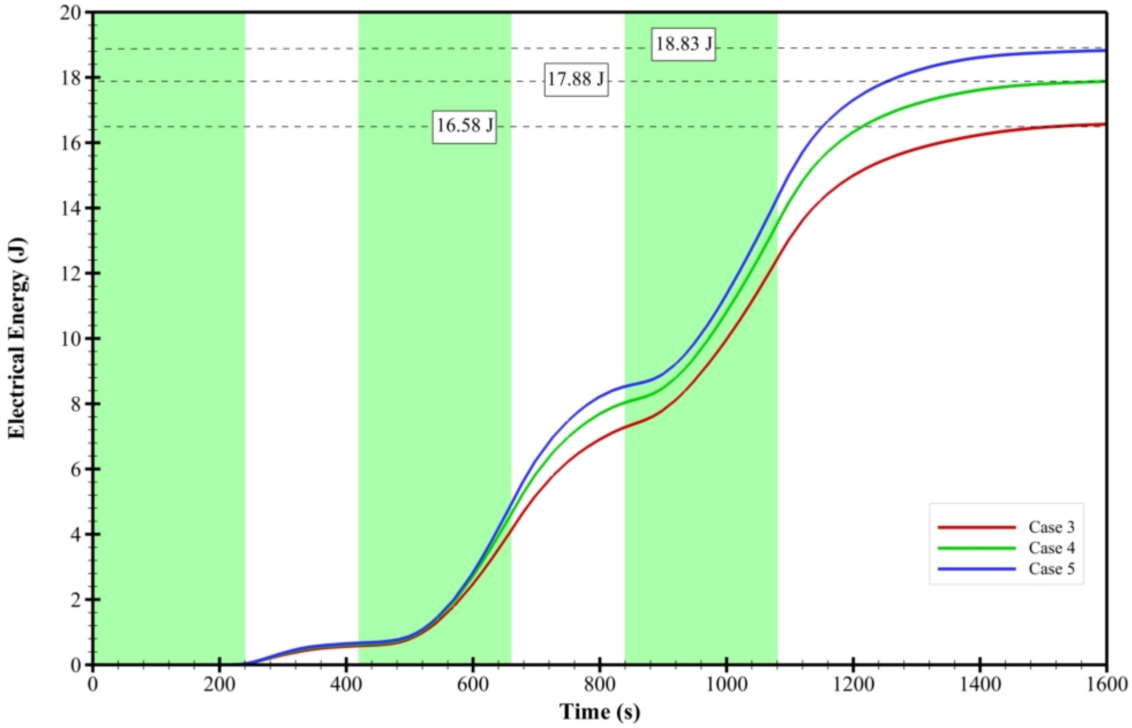

(b)

Fig. 16. Variation of electrical power and energy with time

A similar study was performed for porosities of 0.90 and 0.95 and the comparison of the results are shown below in Fig. 17.

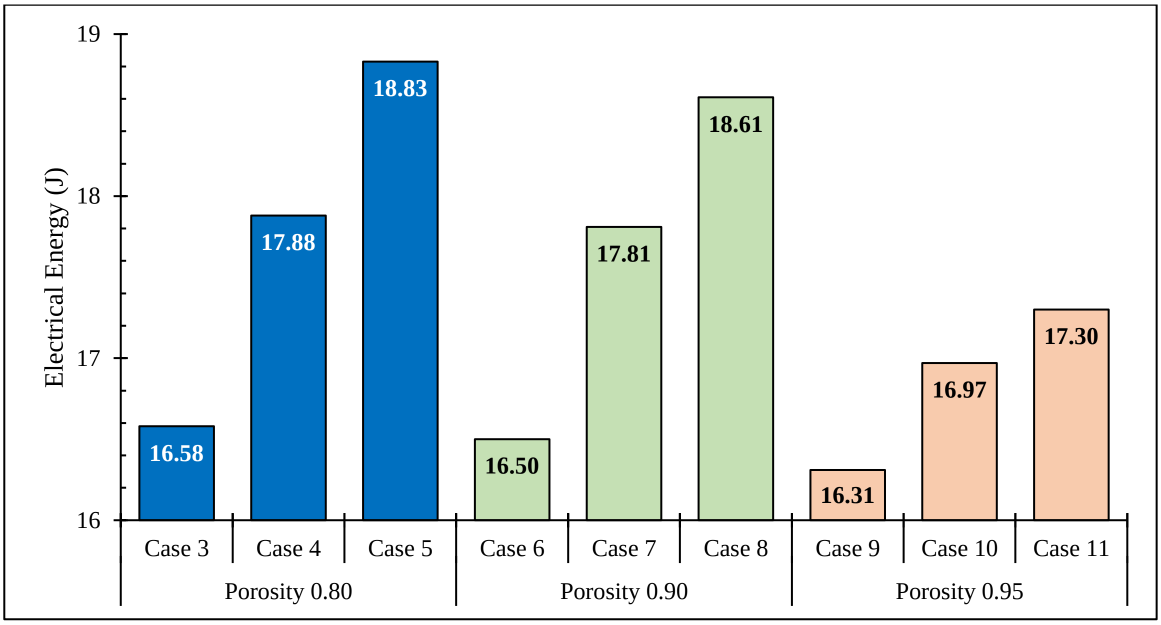

Fig. 17: Effect of changing PPI at constant porosity on electrical energy generation

5.2.2. TEG Performance with Changing of Porosity at Constant PPI

This section provides a detailed analysis of the effect of changes in porosity (at constant PPI) on TEG performance. It should be noted that by changing the porosity, the amount of free space that is filled with paraffin material changes as well. Therefore, as the porosity increases, it increases the amount of PCM and reduces the surface area of the copper plate.

In the following, cases (4, 7, and 10) with PPI of 20 and different porosities will be analysed. Fig. 18 shows the average temperature and liquid fraction of PCM on both sides of the TEG for these cases. As can be seen, both graphs have a completely similar behaviour compared to Fig. 12. Also, it shows in Fig. 18(a) that with increasing the porosity, the average temperature of PCM increases on the hot-side of TEG and decreases on the cold-side. Although the amount of temperature difference is very small it is more visible towards the final seconds of the process. The trend of liquid fraction shown in Fig. 18(b) is also similar to Fig. 12(b). However, by comparing these two figures, it can be seen that changes in porosity have more impact on

TEG performance compared to changes in PPI. The reason for this is that, unlike changes in PPI, when the porosity increases, therefore, more paraffin materials will be used in the system in which, as a result, the time of complete melting will increase as well.

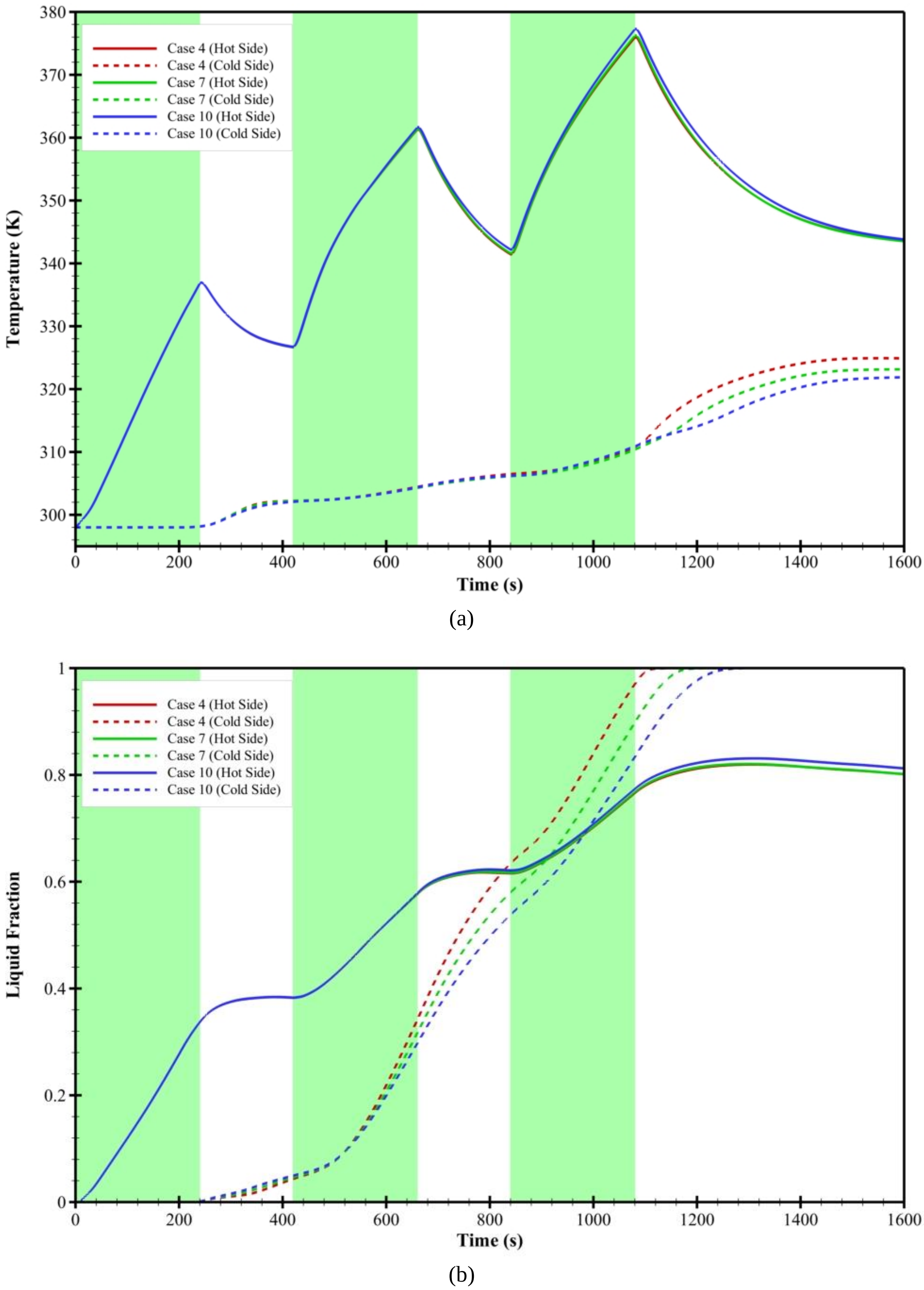

Fig. 18. (a) Variation of the average temperature of PCM with time (b) Variation of the liquid fraction of PCM with time

Fig. 19 shows the variation of heat transfer from PCM in cold-side of the TEG to the heat-sink. Comparing the results with those shown in Fig. 13, it is evident that the increase in porosity is accompanied by a decrease in the rate of heat transfer to the heat-sink. This is because as the porosity increases, the amount of metal foam in copper porous medium decreases thus it reduces the heat transfer.

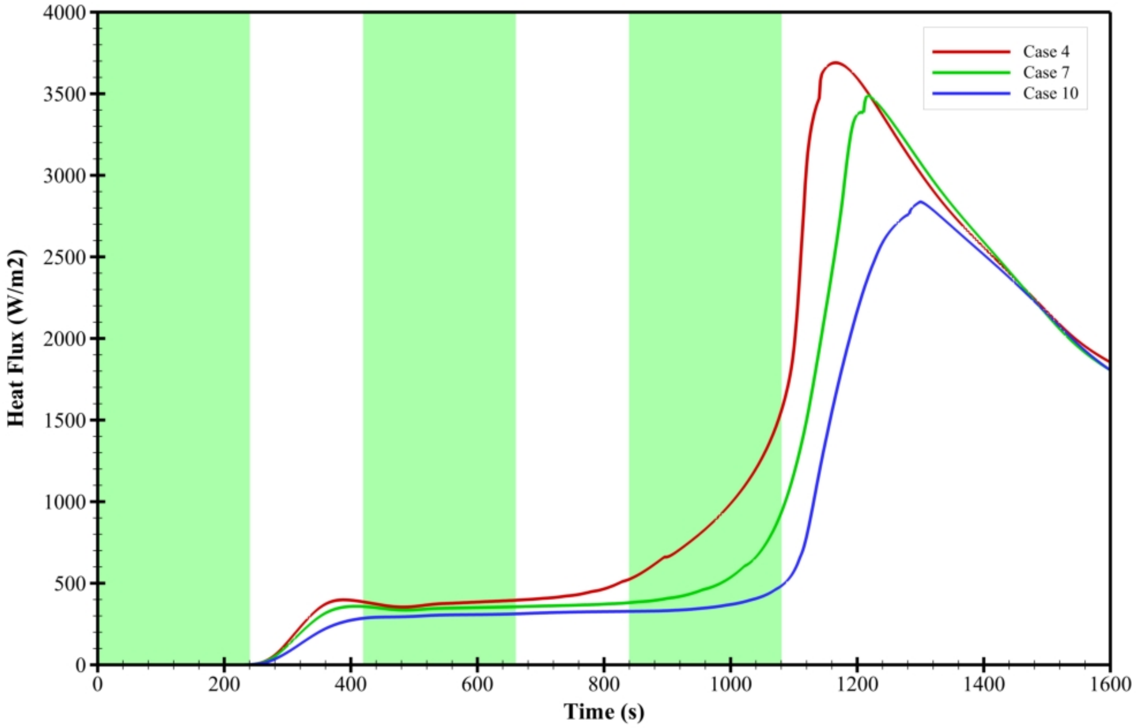

Fig. 19. Variation of heat flux from cold-side PCM to heat-sink with time

A similar comparison can be done with the magnitude of temperature on both sides of the TEG as shown in Fig. 20.

Comparing Fig. 20 and Fig. 14 shows that increasing the porosity has a completely different effect on the temperature of both sides of the TEG and the actual temperature difference, compared to an increase of PPI. As shown in Fig. 20, with increasing porosity in the porous medium, the temperature of the TEG on both sides increases while the temperature difference decreases. The reason for this behaviour is that with increasing the porosity in cold-side of the TEG, the heat conductivity decreases. Therefore, it reduces the heat transfer from the PCM of the cold-side and consequently from the hot-side PCM. This causes the thermal heat confinement on both sides of the TEG, which raises the temperature on both sides. Furthermore, less heat discharge from the cold-side of the TEG will reduce the temperature difference between both sides, respectively.

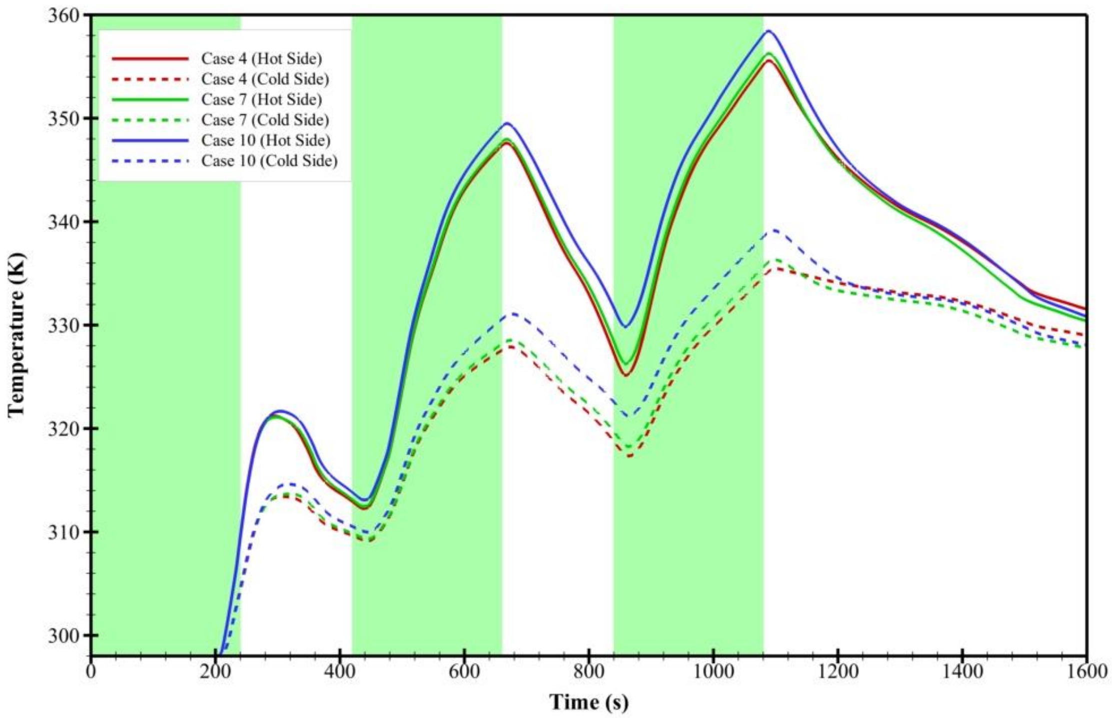

(a)

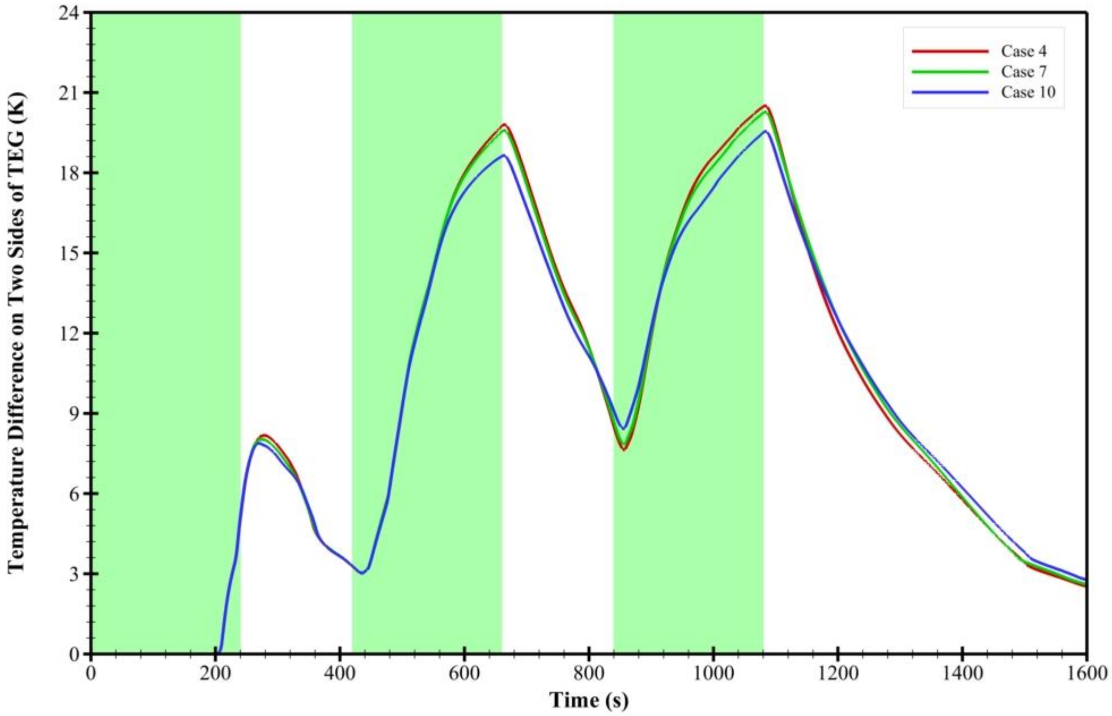

(b)

Fig. 20. Comparison of temperature and its differences between two sides of TEG

The variation of electric voltage generation at different porosities also shows in Fig. 21.

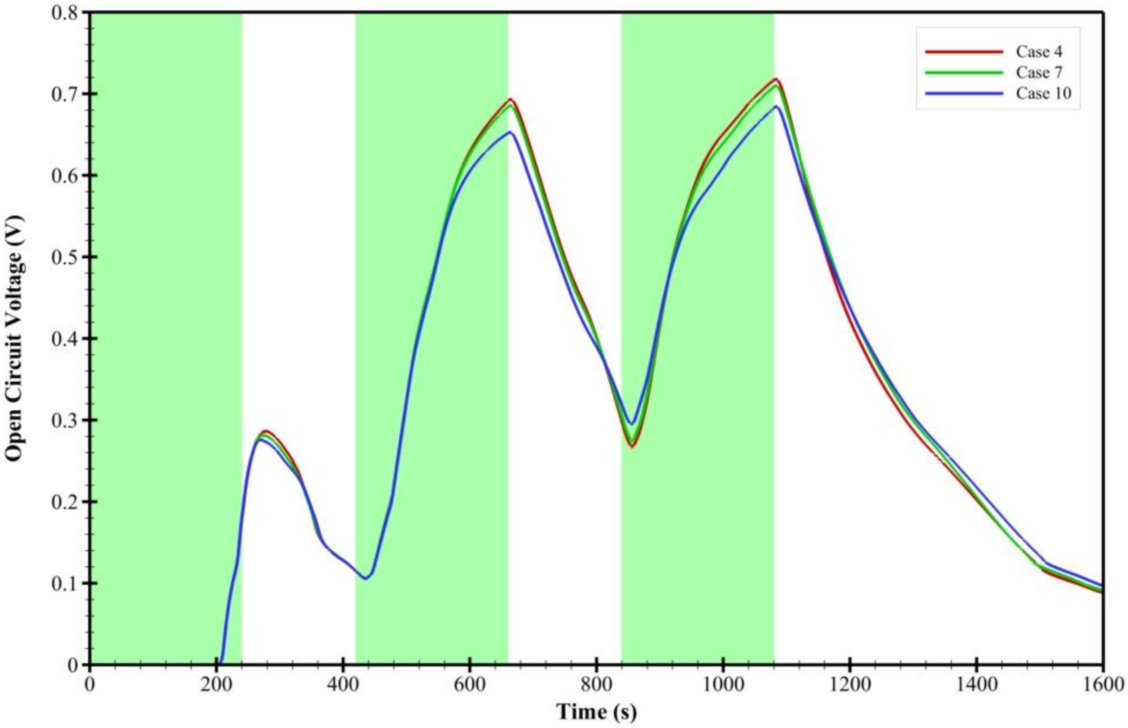

Fig. 21. Variation of electric voltage generation with time

As shown in Fig. 20(b), an increase in temperature reduces the temperature difference between the sides of the TEG. This decrease in temperature difference, according to Fig. 21, leads to a decrease in the electrical voltage generation with TEG, which is related to the electrical power and energy produced. As shown in Fig. 22(b), the amount of electrical energy generated by TEG shows a decrease of 0.4% and 5.7% with an increase in porosity from 0.8 to 0.9 and 0.95, respectively.

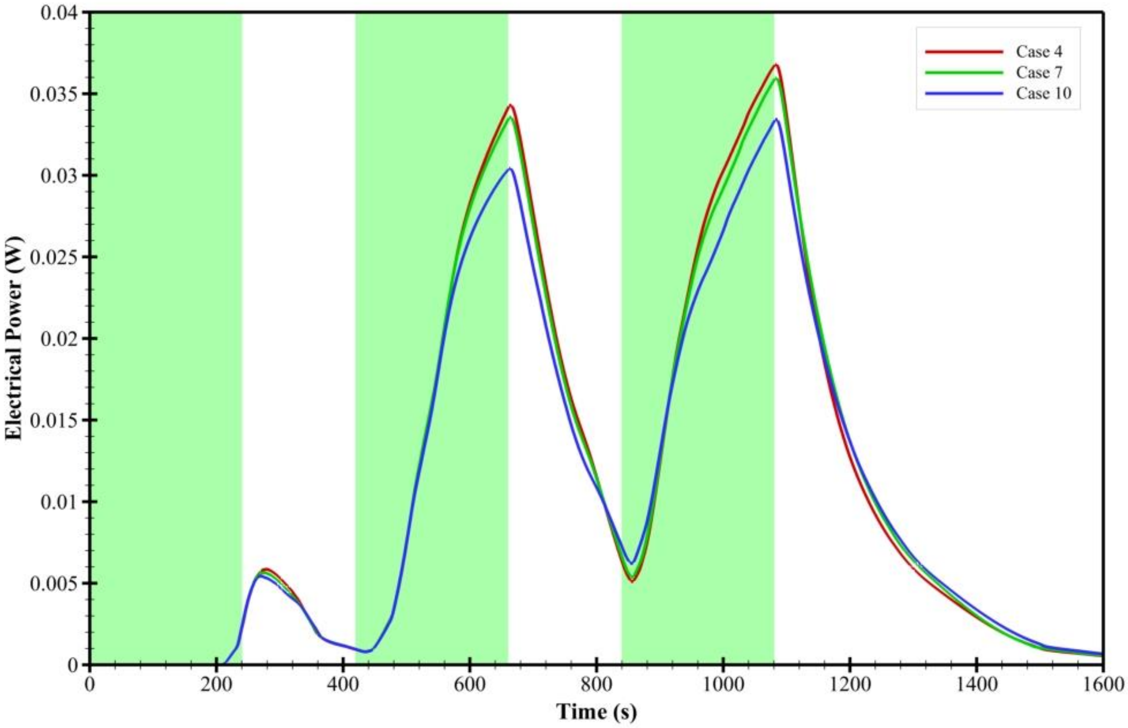

(a)

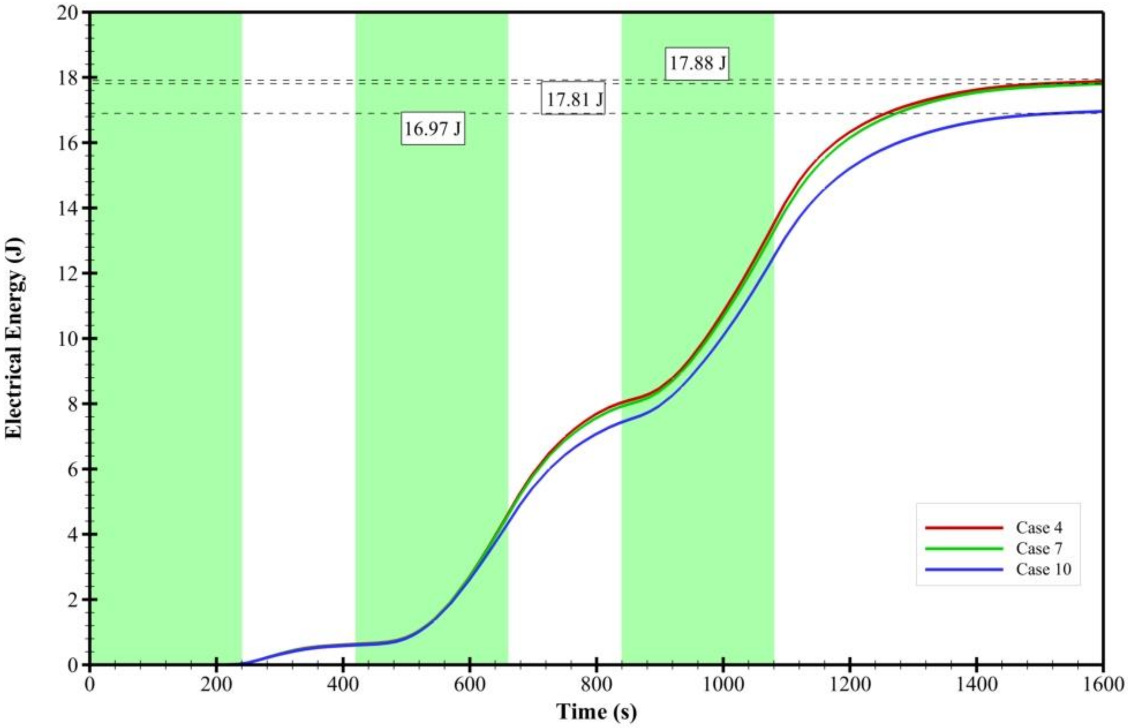

(b)

Fig. 22. Variation of electrical power and energy with time

Fig. 23 shows the bar charts of produced energy in cases with PPI of 10, 20 and 40. As shown in this figure, the changing procedure is similar to cases with PPI of 20.

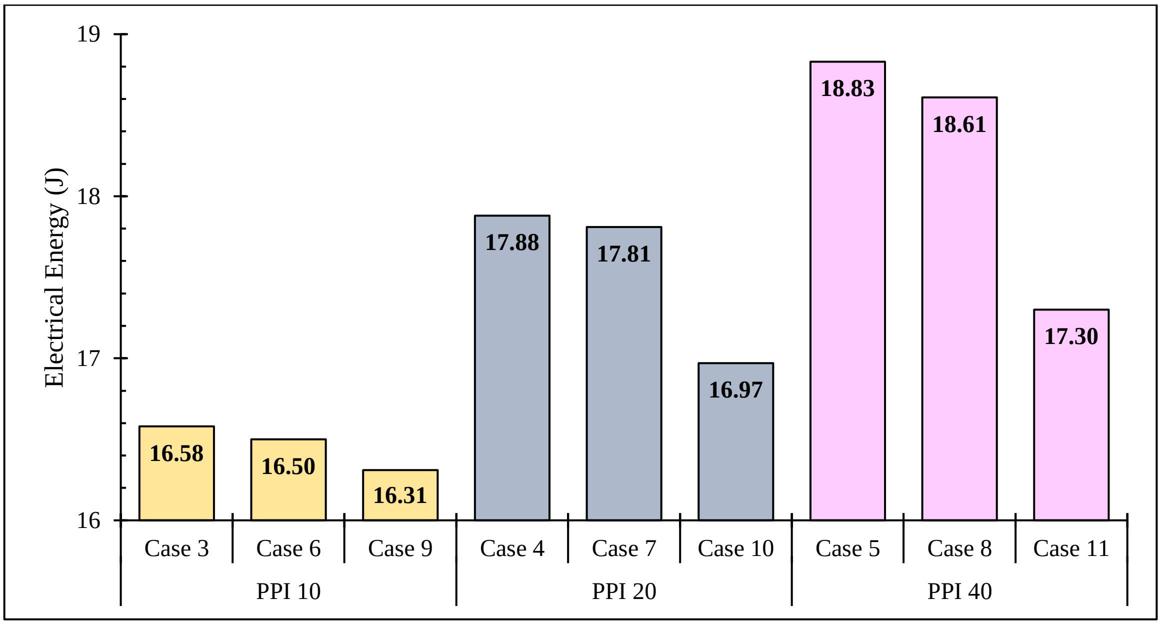

Fig. 13. Effect of changing porosity at constant PPI on electrical energy generation

6. Conclusions

This study shows that, the application of PCM on both sides of the TEG has a positive effect on reducing the fluctuations of output voltage in transient boundary conditions. It also increases the time duration of producing electrical energy when the heat source is cut-off. However, it also has a negative impact in which the output voltage reduces. Therefore, to tackle this problem, the present numerical study, uses a porous medium to increase the efficiency of PCM based thermoelectric harvester and the following results have been obtained:

1. Using porous medium on the cold-side of the TEG improves the system efficiency in terms of output voltage and electrical energy production. The use of a porous medium in cold-side of the TEG with the porosity of 0.80 and PPI of 20 showed an increase in producing electrical energy by 25.47%. Whereas applying porous in the hot-side shows an opposite effect and it reduces the electrical power by 13.33%.

2. Temperature changes and the liquid fraction (due to the melting of PCM) on the hot-side of TEG, are fluctuating, whereas such behaviour is not observed on the cold-side of the thermoelectric generator.
3. The effect of PPI and porosity on system performance is opposite. In overall, the system with high PPI, which is 40 in this study, and low porosity, which is 0.80, shows better efficiency and performance such as heat discharge to heat-sink on the cold-side, producing output voltage and electrical energy.

Nomenclature

A	Area
A_m	Mushy zone constant
A_{sf}	Specific surface area of metal foam (m^2)
C_f	Inertial coefficient
C_p	Specific heat (J/kg.K)
d_l	Ligament diameter (m)
d_p	Pore size (mm)
g	Gravity acceleration (m/s^2)
h	Heat transfer coefficient ($W/m^2 \cdot K$)
h_{sf}	Interfacial heat transfer coefficient ($W/m^2 \cdot K$)
K	Permeability of porous foam (m^2)
k	Thermal conductivity coefficient (W/m.K)
L	latent heat of fusion(J/kg.K)
n	Normal direction of surfaces
P	Pressure (Pa)
Pr	Prandtl number
Q	Thermal energy rate (W)
q''	Heat flux (W/m^2)
R_{in}	Internal electrical resistance of the thermoelectric generator (Ohm)
Re	Reynolds number
T	Temperature (K)
u	Velocity in x-direction (m/s)
v	Velocity in y-direction (m/s)
ZT	Figure of merit

Abbreviations

PCM	Phase Change Material
PPI	Pore Per Inch
TEG	Thermoelectric Generator
RT	Rubitherm Gmbh Germany

Greek symbols

α	Seebeck coefficient (V/K)
β	Thermal expansion coefficient (1/K)

ε	Porosity of the copper foam
λ	Liquid fraction
μ	Dynamic viscosity (kg/m.s)
ρ	Fluid density (kg/m^3)
σ	Electrical conductivity coefficient of TEG (S)
ω	Pore density (PPI)

Subscripts

c	Cold
e	Effective value
f	Fluid
h	Hot
l	Liquid
ref	Reference
s	Solid

References

[1] T. N. Huu, T. N. Van, and O. Takahito, "Flexible thermoelectric power generator with Y-type structure using electrochemical deposition process," *Applied Energy,* vol. 210, pp. 467-476, 2018, doi: http://dx.doi.org/10.1016/j.apenergy.2017.05.005.

[2] Y. J. Kim, H. M. Gu, C. S. Kim, H. Choi, G. Lee, S. Kim, K. Y. Kevin, S. G. Lee, and B. J. Cho, "High-performance self-powered wireless sensor node driven by a flexible thermoelectric generator," *Energy,* vol. 162, pp. 526-533, 2018, doi: https://doi.org/10.1016/j.energy.2018.08.064.

[3] S. Addanki and D. Nedumaran, "Simulation and fabrication of thermoelectric generators for hand held electronic gadgets," *Materials Science and Engineering: B,* vol. 251, p. 114453, 2019, doi: https://doi.org/10.1016/j.mseb.2019.114453.

[4] M. Aljaghtham and E. Celik, "Design optimization of oil pan thermoelectric generator to recover waste heat from internal combustion engines," *Energy,* vol. 200, p. 117547, 2020, doi: https://doi.org/10.1016/j.energy.2020.117547.

[5] Z. Yuan, X. Tang, Z. Xu, J. Li, W. Chen, K. Liu, Y. Liu, and Z. Zhang, "Screen-printed radial structure micro radioisotope thermoelectric generator," *Applied Energy,* vol. 225, pp. 746-754, 2018, doi: https://doi.org/10.1016/j.apenergy.2018.05.073.

[6] N. Jaziri, A. Boughamoura, J. Müller, B. Mezghani, F. Tounsi, and M. Ismail, "A comprehensive review of Thermoelectric Generators: Technologies and common applications," *Energy Reports,* 2019, doi: https://doi.org/10.1016/j.egyr.2019.12.011.

[7] X. Zheng, C. Liu, Y. Yan, and Q. Wang, "A review of thermoelectrics research–Recent developments and potentials for sustainable and renewable energy applications," *Renewable and Sustainable Energy Reviews,* vol. 32, pp. 486-503, 2014, doi: http://dx.doi.org/10.1016/j.rser.2013.12.053.

[8] X. Gou, H. Ping, Q. Ou, H. Xiao, and S. Qing, "A novel thermoelectric generation system with thermal switch," *Applied Energy,* vol. 160, pp. 843-852, 2015, doi: http://dx.doi.org/10.1016/j.apenergy.2014.11.049.

[9] K. Mizuno, K. Sawada, T. Nemoto, and T. Iida, "Development of a thermal buffering device to cope with temperature fluctuations for a thermoelectric power generator," *Journal of electronic materials,* vol. 41, no. 6, pp. 1256-1262, 2012, doi: https://doi.org/10.1007/s11664-012-1911-2.

[10] S. Borhani, M. Hosseini, A. Ranjbar, and R. Bahrampoury, "Investigation of phase change in a spiral-fin heat exchanger," *Applied Mathematical Modelling,* vol. 67, pp. 297-314, 2019, doi: https://doi.org/10.1016/j.apm.2018.10.029.

[11] L. Liu, X. Fan, Y. Zhang, S. Zhang, W. Wang, X. Jin, and B. Tang, "Novel bio-based phase change materials with high enthalpy for thermal energy storage," *Applied Energy,* vol. 268, p. 114979, 2020, doi: https://doi.org/10.1016/j.apenergy.2020.114979.

[12] S.-F. Li, Z.-h. Liu, and X.-J. Wang, "A comprehensive review on positive cold energy storage technologies and applications in air conditioning with phase change materials," *Applied Energy,* vol. 255, p. 113667, 2019, doi: https://doi.org/10.1016/j.apenergy.2019.113667.

[13] R. Zeinelabdein, S. Omer, and G. Gan, "Critical review of latent heat storage systems for free cooling in buildings," *Renewable and Sustainable Energy Reviews,* vol. 82, pp. 2843-2868, 2018, doi: http://dx.doi.org/10.1016/j.rser.2017.10.046.

[14] R. Pakrouh, M. Hosseini, A. Ranjbar, and R. Bahrampoury, "A numerical method for PCM-based pin fin heat sinks optimization," *Energy Conversion and Management,* vol. 103, pp. 542-552, 2015, doi: http://dx.doi.org/10.1016/j.enconman.2015.07.003.

[15] Q. Ren, P. Guo, and J. Zhu, "Thermal management of electronic devices using pin-fin based cascade microencapsulated PCM/expanded graphite composite," *International Journal of Heat and Mass Transfer,* vol. 149, p. 119199, 2020, doi: https://doi.org/10.1016/j.ijheatmasstransfer.2019.119199.

[16] A. A. Ananno, M. H. Masud, P. Dabnichki, and A. Ahmed, "Design and numerical analysis of a hybrid geothermal PCM flat plate solar collector dryer for developing countries," *Solar Energy,* vol. 196, pp. 270-286, 2020, doi: https://doi.org/10.1016/j.solener.2019.11.069.

[17] M. Eisapour, A. H. Eisapour, M. Hosseini, and P. Talebizadehsardari, "Exergy and energy analysis of wavy tubes photovoltaic-thermal systems using microencapsulated PCM nano-slurry coolant fluid," *Applied Energy,* vol. 266, p. 114849, 2020, doi: https://doi.org/10.1016/j.apenergy.2020.114849.

[18] S. A. Atouei, A. A. Ranjbar, and A. Rezania, "Experimental investigation of two-stage thermoelectric generator system integrated with phase change materials," *Applied energy,* vol. 208, pp. 332-343, 2017, doi: http://dx.doi.org/10.1016/j.apenergy.2017.10.032.

[19] S. A. Atouei, A. Rezania, A. Ranjbar, and L. A. Rosendahl, "Protection and thermal management of thermoelectric generator system using phase change materials: An experimental investigation," *Energy,* vol. 156, pp. 311-318, 2018, doi: https://doi.org/10.1016/j.energy.2018.05.109.

[20] Y. Tu, W. Zhu, T. Lu, and Y. Deng, "A novel thermoelectric harvester based on high-performance phase change material for space application," *Applied energy,* vol. 206, pp. 1194-1202, 2017, doi: http://dx.doi.org/10.1016/j.apenergy.2017.10.030.

[21] W. Zhu, Y. Tu, and Y. Deng, "Multi-parameter optimization design of thermoelectric harvester based on phase change material for space generation," *Applied energy,* vol. 228, pp. 873-880, 2018, doi: https://doi.org/10.1016/j.apenergy.2018.06.151.

[22] M. Araiz, A. Martínez, D. Astrain, and P. Aranguren, "Experimental and computational study on thermoelectric generators using thermosyphons with phase change as heat exchangers," *Energy Conversion and Management*, vol. 137, pp. 155-164, 2017, doi: http://dx.doi.org/10.1016/j.enconman.2017.01.046.

[23] T. Cui, Y. Xuan, E. Yin, Q. Li, and D. Li, "Experimental investigation on potential of a concentrated photovoltaic-thermoelectric system with phase change materials," *Energy*, vol. 122, pp. 94-102, 2017, doi: http://dx.doi.org/10.1016/j.energy.2017.01.087.

[24] M. Jaworski, M. Bednarczyk, and M. Czachor, "Experimental investigation of thermoelectric generator (TEG) with PCM module," *Applied Thermal Engineering*, vol. 96, pp. 527-533, 2016, doi: http://dx.doi.org/10.1016/j.applthermaleng.2015.12.005.

[25] C. Selvam, S. Manikandan, N. V. Krishna, R. Lamba, S. Kaushik, and O. Mahian, "Enhanced thermal performance of a thermoelectric generator with phase change materials," *International Communications in Heat and Mass Transfer*, vol. 114, p. 104561, 2020, doi: https://doi.org/10.1016/j.icheatmasstransfer.2020.104561.

[26] X. Liao, Y. Liu, J. Ren, L. Guan, X. Sang, B. Wang, H. Zhang, Q. Wang, and T. Ma, "Investigation of a double-PCM-based thermoelectric energy-harvesting device using temperature fluctuations in an ambient environment," *Energy*, vol. 202, p. 117724, 2020, doi: https://doi.org/10.1016/j.energy.2020.117724.

[27] T. Rehman, H. M. Ali, M. M. Janjua, U. Sajjad, and W.-M. Yan, "A critical review on heat transfer augmentation of phase change materials embedded with porous materials/foams," *International Journal of Heat and Mass Transfer*, vol. 135, pp. 649-673, 2019, doi: https://doi.org/10.1016/j.ijheatmasstransfer.2019.02.001.

[28] "PCM RT-LINE: Wide-ranging organic PCM for your application." https://www.rubitherm.eu/en/index.php/productcategory/organische-pcm-rt (accessed: 2020).

[29] A. Brent, V. R. Voller, and K. Reid, "Enthalpy-porosity technique for modeling convection-diffusion phase change: application to the melting of a pure metal," *Numerical Heat Transfer, Part A Applications*, vol. 13, no. 3, pp. 297-318, 1988, doi: http://dx.doi.org/10.1080/10407788808913615.

[30] Y. Xu, M.-J. Li, Z.-J. Zheng, and X.-D. Xue, "Melting performance enhancement of phase change material by a limited amount of metal foam: Configurational optimization and economic assessment," *Applied energy*, vol. 212, pp. 868-880, 2018, doi: https://doi.org/10.1016/j.apenergy.2017.12.082.

[31] E. A. Spiegel and G. Veronis, "On the Boussinesq approximation for a compressible fluid," *The Astrophysical Journal*, vol. 131, pp. 442-447, 1960, doi: https://doi.org/10.1086/146849.

[32] Z.-G. Wu, W.-C. Sheng, W.-Q. Tao, and Z. Li, "A novel experimental-numerical method for studying the thermal behaviors of phase change material in a porous cavity," *Solar Energy*, vol. 169, pp. 325-334, 2018, doi: https://doi.org/10.1016/j.solener.2018.05.014.

[33] J. M. Mahdi and E. C. Nsofor, "Melting enhancement in triplex-tube latent heat energy storage system using nanoparticles-metal foam combination," *Applied Energy*, vol. 191, pp. 22-34, 2017, doi: http://dx.doi.org/10.1016/j.apenergy.2016.11.036.

[34] A. V. Arasu and A. S. Mujumdar, "Numerical study on melting of paraffin wax with Al2O3 in a square enclosure," *International Communications in Heat and Mass Transfer*, vol. 39, no. 1, pp. 8-16, 2012, doi: http://dx.doi.org/10.1016/j.icheatmasstransfer.2011.09.013.

[35] V. V. Calmidi and R. L. Mahajan, "Forced convection in high porosity metal foams," *J. Heat Transfer*, vol. 122, no. 3, pp. 557-565, 2000, doi: https://doi.org/10.1115/1.1287793.

[36] Y. Tian and C.-Y. Zhao, "A numerical investigation of heat transfer in phase change materials (PCMs) embedded in porous metals," *Energy*, vol. 36, no. 9, pp. 5539-5546, 2011, doi: http://dx.doi.org/10.1016/j.energy.2011.07.019.

[37] A. Zukauskas, "Heat transfer from tubes in crossflow," *Advances in heat transfer*, vol. 18, no. 1, pp. 87-159, 1987, doi: https://doi.org/10.1016/S0065-2717(08)70118-7.

[38] H. F. Kohan, F. Lotfipour, and M. Eslami, "Numerical simulation of a photovoltaic thermoelectric hybrid power generation system," *Solar Energy*, vol. 174, pp. 537-548, 2018, doi: https://doi.org/10.1016/j.solener.2018.09.046.

[39] H. Lee, *Thermoelectrics: design and materials*. John Wiley & Sons, 2016, doi: https://doi.org/10.1002/9781118848944.

[40] S. V. Patankar, *Numerical heat transfer and fluid flow*. CRC Press, 1980, doi: https://doi.org/10.1201/9781482234213.

[41] J. H. Ferziger, M. Perić, and R. L. Street, *Computational methods for fluid dynamics*. Springer, 2002, doi: https://doi.org/10.1007/978-3-642-56026-2.

[42] P. Zhang, Z. Meng, H. Zhu, Y. Wang, and S. Peng, "Melting heat transfer characteristics of a composite phase change material fabricated by paraffin and metal foam," *Applied Energy*, vol. 185, pp. 1971-1983, 2017, doi: http://dx.doi.org/10.1016/j.apenergy.2015.10.075.